ESA CONTRACT REPORT

Contract Report to the European Space Agency

SMOS Neural Network Soil Moisture Data Assimilation

N.J. Rodríguez-Fernández, P. de Rosnay, C. Albergel, F. Aires, C. Prigent, P. Richaume, Y.H. Kerr, J. Muñoz-Sabater

Progress report for ESA contract
4000101703/10/NL/FF/fk

European Centre for Medium-Range Weather Forecasts
Europäisches Zentrum für mittelfristige Wettervorhersage
Centre européen pour les prévisions météorologiques à moyen terme

ECMWF

Series: ECMWF ESA Project Report Series

A full list of ECMWF Publications can be found on our web site under:
http://www.ecmwf.int/en/research/publications

Contact: library@ecmwf.int

European Centre for Medium Range Weather Forecasts
Shinfield Park, Reading, RG2 9AX, England

Contract Report to the European Space Agency

SMOS Neural Network Soil Moisture Data Assimilation

Authors: N.J. Rodríguez-Fernández, P. de Rosnay, C. Albergel, F. Aires[2], C. Prigent[2], P. Richaume[1], Y.H. Kerr[1], J. Muñoz-Sabater

Progress report for ESA contract 4000101703/10/NL/FF/fk

[1] CESBIO (CNRS, CNES, IRD, Université Paul Sabatier), 18 av. Edouard Belin, bpi 2801, 31401 Toulouse cedex 9, France
[2] Estellus, Observatoire de Paris

January 2017

	Name	Company
First version prepared by (October 2016)		ECMWF
Quality Visa		ECMWF
Application Authorized by		ESA/ESRIN

Distribution list:

ESA/ESRIN
Susanne Mecklenburg
ESA ESRIN Documentation Desk

ESA/ESTEC
Technical Officer: Matthias Drusch

ECMWF
Stephen English

Contents

Abstract

A set of Soil Moisture and Ocean Salinity (SMOS) soil moisture (SM) data assimilation (DA) experiments are presented. The SMOS soil moisture dataset used in this study was produced specifically for this project training a neural network (NN) using SMOS brightness temperatures as input and H-TESSEL SM fields as reference for the training. In this way, the SMOS NN SM dataset has a similar climatology to the model and it does not present a global bias with respect to the model. The DA experiments are computed using a surface-only Land Data Assimilation System (so-LDAS) based on the HTESSEL land surface model. This system is very efficient computationally and allows to perform long surface assimilation experiments (one whole year, 2012). SMOS NN SM DA experiments are compared to Advanced Scatterometer (ASCAT) SM DA. In both cases, experiments with and without 2 metre air temperature and relative humidity DA are discussed using different observation errors for the ASCAT and SMOS datasets. Seasonal, geographical and soil-depth-related differences between the results of those experiments are presented and discussed. The different SM analysed fields are evaluated against a large number of in situ measurements of SM. On average, the SM analysis gives in general similar results to the model open loop with no assimilation even if significant differences can be seen for some sites with in situ measurements. The sensitivity to observation errors to the SM dataset slightly differ depending on the networks of in situ measurements, however it is relatively low for the tests conducted here. Finally, the effect of the soil moisture analysis on the Numerical Weather Prediction (NWP) is evaluated comparing experiments for different configurations of the system, with and without (Open Loop) soil moisture data assimilation. Assimilation of ASCAT soil moisture improves the forecast in the tropics and adds information with respect to the near surface conventional observations. In contrast, SMOS degrades the forecast in the Tropics in July-September. In the Southern hemisphere ASCAT degrades the forecast in July-September both alone and using 2m air temperature and relative humidity. On the other hand, experiments using SMOS (even without screen level variables) improve the forecast for all the seasons, in particular, in July-December. In the Northern Hemisphere both with ASCAT and SMOS, the experiments using 2m air temperature and relative humidity improve the forecast in April-September. SMOS alone has a significant positive effect in July-September for experiments with low observation error. Maps of the forecast skill with respect to the open loop experiment show that SMOS improves the forecast in North America and to a lesser extent in Northern Asia for up to 72 hours.

1 Introduction

The amount of moisture in the soil is an important variable to understand the coupling of the continental surface and the atmosphere (Koster et al., 2004; Tuttle and Salvucci, 2016). Soil moisture initialization is also crucial in seasonal forecasting studies, since anomalies may persist at monthly to seasonal time scales (Seneviratne et al., 2010). Mahfouf (1991) showed that it is possible to analyse soil moisture using near-surface parameters such as the so-called screen level variables (SLV: 2m air temperature, T_{2m}, and relative humidity, RH_{2m}). Using an optimal interpolation (OI) approach it was shown that it is possible to improve the boundary-layer forecasts skill (Mahfouf et al., 2000; Douville et al., 2000). Other soil moistures analysis schemes were evaluated by Balsamo et al. (2004) and Mahfouf et al. (2009), for instance. Balsamo et al. (2004) used a two-dimensional variational (2D-VAR) analysis of soil moisture from screen level observations in a mesoscale weather-prediction model. They showed that the 2D-VAR analysis is more robust than the OI soil moisture analysis, which is strongly driven by the assimilated observations, leading to high spatial and temporal variability. This approach was used to study the information content of SLVs and microwave observations in the context of the Canadian Land Data Assimilation System (Balsamo et al., 2007). Mahfouf et al. (2009) used an off-line version of the Interaction between Soil Biosphere and Atmosphere (ISBA, Noilhan and Planton, 1989; Noilhan and Mahfouf, 1996) land surface model for the initialization of soil water content and temperature in numerical weather prediction (NWP) models. They compared a soil analysis based on OI of SLVs to a soil analysis with a simplified version of the Extended Kalman Filter (hereafter SEKF), which keeps the covariance matrix of background errors constant. The two soil analysis schemes showed a similar response to screen level atmospheric errors but the SEKF approach was shown to be superior in identifying situations where the near-surface atmosphere is

sensitive to soil perturbations, leading to better use of observations. Drusch et al. (2009) also showed that an EKF analysis gives soil moisture increments as a function of soil depth more realistic than those obtained using OI. An additional advantage of the SEKF approach is that it allows an easier assimilation of satellite observations (Mahfouf et al., 2009). Therefore, the OI soil moisture analysis at ECMWF was replaced by an SEKF (de Rosnay et al., 2013). The performance was evaluated on soil moisture, 2 m air temperature and relative humidity, and showed a consistent improvement on screen-level parameters and soil moisture forecasts with respect to the OI analysis.

Since T_{2m} and RH_{2m} are not always representative of the soil moisture (SM) content it is also interesting to assimilate directly SM information. Local studies have shown the interest of assimilating in situ measurements of SM (Parrens et al., 2014). However, SM in situ measurements are too scarce to be used in a global SM analysis system. Remote sensing datasets do not show this limitation. Drusch (2007) studied the assimilation of TMI (TRMM Microwave Imager) SM trough a nudging scheme. They showed that the SM analysis gives the most accurate estimate when compared against *in situ* observations from the Oklahoma Mesonet and that it influences local weather parameters including the planetary boundary layer height and cloud coverage. Draper et al. (2009) studied the assimilation of ASMR-E soil moisture into the ISBA model both with an EKF and an SEKF, which produced similar SM analysis. In preparation to the assimilation of the MetOp Advanced Scatterometer (ASCAT) SM index, Scipal et al. (2008) used the nudging scheme with data from its predecessor instruments, the ERS-1/2 scatterometers. They compared the results from this experiment against those from a control experiment where SM evolved freely and against those from the then operational ECMWF forecast system with OI of SLV to analyse SM. Validation against field observations from the Oklahoma Mesonet, showed that the assimilation of ERS SM index increased the correlation (and decreased the Root Mean Square Error) significantly. The corresponding forecasts for low level temperature and humidity improved only marginally compared to the control experiment and showed a decrease of performances compared to the OI analysis using SLV. They suggested that a more advanced data assimilation system, like an EKF, could use the satellite observations more efficiently. This was done by de Rosnay et al. (2013), who included an SEKF analysis of T_{2m}, RH_{2m} and soil moisture index from ASCAT. This is the current operational system at ECMWF. Results with ASCAT data assimilation show a neutral impact on both soil moisture and screen-level parameters (de Rosnay et al., 2013).

An alternative to analyse soil moisture is to assimilate an observable directly related to soil moisture such as microwave brightness temperatures (T_b's). One advantage of assimilating T_b's is that they have well-defined associated uncertainties and that they can be easily available in near-real-time (NRT), which make it possible their use in an operational system. For instance, Seuffert et al. (2004) studied the assimilation of aircraft T_b's in addition to T_{2m} and RH_{2m}. They showed that performing a joint assimilation gives more consistent results than assimilating T_b's and SLV separately.

The launch of the Soil Moisture and Ocean Salinity (SMOS) satellite (Kerr et al., 2010) in November 2009 has made available global L-band (1.4 GHz) observations in polarimetry mode with multi-angular capabilities and a revisit time of three days or less. SMOS T_b's are available in NRT since the beginning of the mission (Gutierrez and Canales Molina, 2010; de Rosnay et al., 2012). The assimilation of SMOS T_b's into the ECMWF Integrated Forecast System (IFS) is a complex task. An observation operator going from soil moisture to multi-angular and dual-polarization brightness temperature in the top of the atmosphere has to be implemented. The radiative transfer is done with the Community Microwave Emission Model (CMEM, de Rosnay et al., 2009). The T_b's assimilation strategy has been described by Muñoz-Sabater (2015). Other weather prediction centres are also working towards the same goal (Carrera et al., 2016). In addition, the assimilation of SMOS T_b's has also been used to constrain hydrological models (De Lannoy and Reichle, 2016; Lievens et al., 2016).

Other studies have investigated the assimilation of SMOS SM instead of the T_b's. For instance SMOS SM has been assimilated into a land surface-hydrological model, Modélisation Environmentale Surface et Hydrologie (MESH), over the Great Lakes basin (Xu et al., 2015), into the Noah Land Surface Model of the NASA

Land Information System (Blankenship et al., 2016), into SVAT (Soil Vegetation Atmosphere Transfer) models (Martens et al., 2016; Ridler et al., 2014) and in carbon-cycle models (Scholze et al., 2016). The two approaches, the assimilation of SMOS SM or SMOS T_b's via CMEM, were compared by Lievens et al. (2016) using the Variable Infiltration Capacity (VIC) hydrological model. The best results were achieved from assimilation of the SM measurements. They interpreted this result as a consequence of the difficulty to model and to bias correct the radiative transfer with CMEM.

In the context of the assimilation of soil moisture data, the considered observations need to be re-scaled to remove any bias and to be consistent with the model climatology (e.g., Drusch et al., 2005; de Rosnay et al., 2013). This can be done *a posteriori* by matching the Cumulative Density Function (CDF) of both datasets. In addition, as already mentioned, assimilating T_b's requires to perform approximate radiative transfer computations to implement an observation operator. Aires et al. (2005) and Aires and Prigent (2006) proposed an alternative approach. They showed that it is possible to use neural networks (NNs) to link observables such as microwave T_b's or backscattering coefficients to global soil moisture fields, in particular from numerical weather prediction models. Rodríguez-Fernández et al. (2015) showed that it is possible to use this technique also with SMOS. Since a NN already trained is very fast to apply, the European Space Agency decided to use this approach to implement an SMOS NRT SM processor (Rodríguez-Fernández et al., 2016; Muñoz-Sabater et al., 2016b; Mecklenburg et al., 2016). Another interesting property of the NN SM retrievals is that, by construction, they share most of the statistical properties with the model SM dataset used as reference for the training phase. For instance, they do not have a global bias with respect to the reference SM dataset and both datasets show a similar climatology. Therefore, Aires et al. (2005) and Aires and Prigent (2006) proposed this methodology to compute SM fields for an efficient data assimilation.

The goal of this study is to perform data assimilation (DA) experiments to analyse SM using a SMOS SM dataset obtained with a NN trained on ECMWF IFS models. These DA experiments were compared to DA of ASCAT soil moisture index after CDF matching, to the assimilation of T_{2m} and RH_{2m} and to a control experiment where the model SM is not re-initialized with a SM analysis (hereafter "open-loop"). The rest of this document organized as follows. Section 2 describes the observational datasets to be assimilated (SMOS NN SM, ASCAT SM, SLVs) and the in situ measurements used for evaluation. Section 3 discusses the DA framework used. Section 4 shows the results of the analysis of SM using SLVs, SMOS NN SM, ASCAT SM with different observation errors. The impact of the DA on SM and on atmospheric forecasts are presented in Sections 5.1 and 5.2, respectively. Finally, Section 6 summarizes the results and the conclusions.

2 Data

2.1 HTESSEL and ERA-Interim/Land models

The land surface model used in this study is the "Tiled ECMWF Scheme for Surface Exchanges over Land" (TESSEL) (van den Hurk et al., 2000) with improved land surface hydrology (H-TESSEL) (Balsamo et al., 2009). The impact of HTESSEL is a reduction in baseflow compared to TESSEL, which had virtually zero surface runoff in unfrozen conditions (Balsamo et al., 2010). The new soil hydrology has been shown to affect the quality of seasonal prediction in extreme events associated to soil moisture-precipitation feedback as the European summer heatwave in 2003 (Weisheimer et al., 2011). A significant revision of the snow parametrisation used in H-TESSEL took place in 2009 with the improvement of the thermal energy exchange with a substantial reduction of near-surface temperature errors in snow-dominated areas. In November 2010 H-TESSEL was further improved by implementing a monthly varying climatology of leaf area index (LAI) based on MODIS data (Boussetta et al., 2013) that replaces a fixed maximum LAI and that has shown a reduction of near-surface temperature errors in the tropical and mid-latitude areas particularly evident in spring and summer.

Table 1: In situ networks used in this study. The depths are quoted as two numbers: the first one is the upper depth, and the second one is the lower depth of the sensor. Both numbers are equal when the sensor is placed horizontally. The third column gives the number of sensors remaining for each network after applying all of the criteria used for the evaluation that are discussed in Section 2.5. The third column gives the average number of points in the times series for each network that satisfies the evaluation criteria.

Network	Depth (cm)	Sites	Points	Location	Reference
DAHRA	0.05–0.05	1	492	Senegal	Tagesson et al. (2015)
REMEDHUS	0.00–0.05	25	988	Spain	Martínez-Fernández and Ceballos (2005)
SMOSMANIA	0.05–0.05	14	576	France	Calvet et al. (2007)
HOBE	0.00–0.05	46	687	Denmark	Bircher et al. (2012, 2013)
PERUGIA	0.05–0.05	2	719	Italy	
FMI	0.05–0.05	8	245	Finland	
SCAN	0.05–0.05	88	588	USA	Schaefer et al. (2007)
SNOTEL	0.05–0.05	147	459	USA	Leavesley et al. (2008)
USCRN	0.05–0.05	122	931	USA	
ARM	0.05–0.05	38	687	USA	
PBO-H2O	0.00–0.05	101	206	USA	
CTP-SMTMN	0.00–0.05	33	365	China	

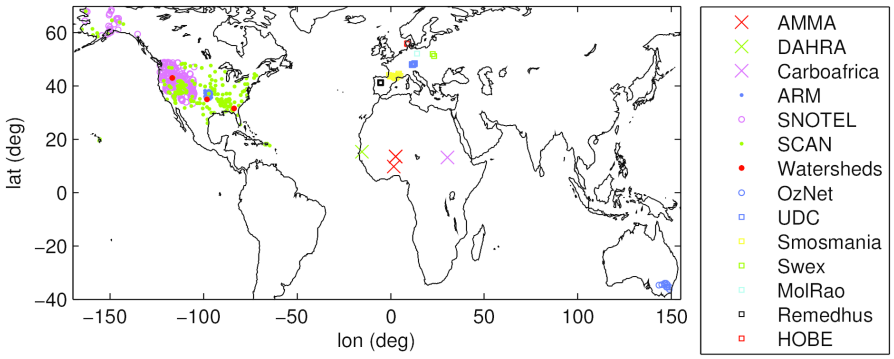

Figure 1: Location of some of the in situ sensors used in the current study.

The bare ground evaporation was also revised by Albergel et al. (2012).

H-TESSEL uses four soil layers. The depths of the soil layers are in an approximate geometric relation (7 cm for the top layer and then 21, 72, and 189 cm). The ECMWF Integrated Forecast System (IFS) uses a spectral representation of meteorological fields where each field is expanded in series of spherical harmonics. The spatial resolution is determined by the truncation of the serie at a given total wavenumber. In this study, the model was run with a spectral truncation T511, since the equivalent spatial resolution of approximately 39 km is similar to that of ASCAT and SMOS. Following the ERA-Interim/Land (Balsamo et al., 2015) approach, H-TESSEL was forced with the near surface atmospheric fields obtained from the ERA-Interim re-analysis (Dee et al., 2011).

2.2 Conventional observations

SYNOP measurements of T_{2m} and RH_{2m} also called screen level observations, are used by NWP centers to analyse their soil moisture. A screen level analysis is performed, providing gridded fields of analysed T_{2m} and RH_{2m} (Mahfouf et al., 2000). The latter are used as input of the soil moisture analysis as detailed in the

overview papers by de Rosnay et al. (2014) and Mahfouf et al. (2009)

2.3 ASCAT moisture index

The C-band (5 GHz) scatterometer ASCAT was launched onboard MetOp in 2006. The EUMETSAT (European Organisation for the Exploitation of Meteorological Satellites) ASCAT surface soil moisture product is the first operational soil moisture product based on satellite data (Bartalis et al., 2007). It is available in near-real time on EUMETCast (which is the EUMETSAT near-real-time dissemination system) and it has been monitored operationally at ECMWF since September 2009. This SM dataset is currently assimilated in the IFS (de Rosnay et al., 2013).

The scatterometer provides a soil moisture index based in the change of the radar back-scattering coefficient at a fixed location. In order to transform this index into volumetric soil moisture. A CDF-matching has been used to match the mean and the variance of H-TESSEL. The CDF-matching performs a bias correction and the output dataset units are volumetric soil moisture as in the model. It is computed as follows:

$$SM_{ASCAT} = a + b \times SMI_{ASCAT}, \tag{1}$$

where SM_{ASCAT} and SMI_{ASCAT} are the ASCAT soil moisture and soil moisture index, respectively, while a and b are the CDF coefficients. The coefficients have been computed on each model grid point independently for each of the twelve months as follows:

$$b = \sigma_{model} / \sigma SMI_{ASCAT} \tag{2}$$

and

$$a = SM_{model} - SMI_{ASCAT} \times b \tag{3}$$

The complete description of the CDF-mathching approach can be found in de Rosnay et al. (2011).

Data from the year 2012 has been used in this study. The ASCAT 25km sampling product available on EUMETCAST is used at ECMWF. The product includes, for each observation, a noise level information, which indicates the product error. It is used to define ASCAT observation error in the set of data assimilation experiments conducted in this paper as shown in Table 2. As part of the quality control the ASCAT soil moisture product is not used for grid points with a topographic complexity larger than 20 % and water fraction larger than 15%.

2.4 SMOS Neural Network Soil Moisture

The SMOS soil moisture dataset used was produced specifically for this study following the approach of Rodríguez-Fernández et al. (2015). The French CATDS (Centre Aval de Traitement de Données SMOS) brightness temperature product (L3TB) (Kerr et al., 2013) was used as input to the neural network because the T_b's are provided averaged in angle bins of 5° width and with polarizations referred to the Earth reference system (horizontal and vertical, H and V) in contrast to the ESA level 2 product, which is not binned and with polarizations expressed in the antenna reference frame.

As for the neural network ESA product (Rodríguez-Fernández et al., 2016) only incidence angles from 30° to 45° have been used in order to maximize the swath width of the retrieval and the quantity of data available for assimilation. Rodríguez-Fernández et al. (2015) showed that adding more information in addition to SMOS T_b's as input to the NN improves its ability to capture the dynamics of the H-TESSEL dataset. It is particularly helpful to add as input the soil texture (clay and sand fractions) or soil moisture linear expectations computed

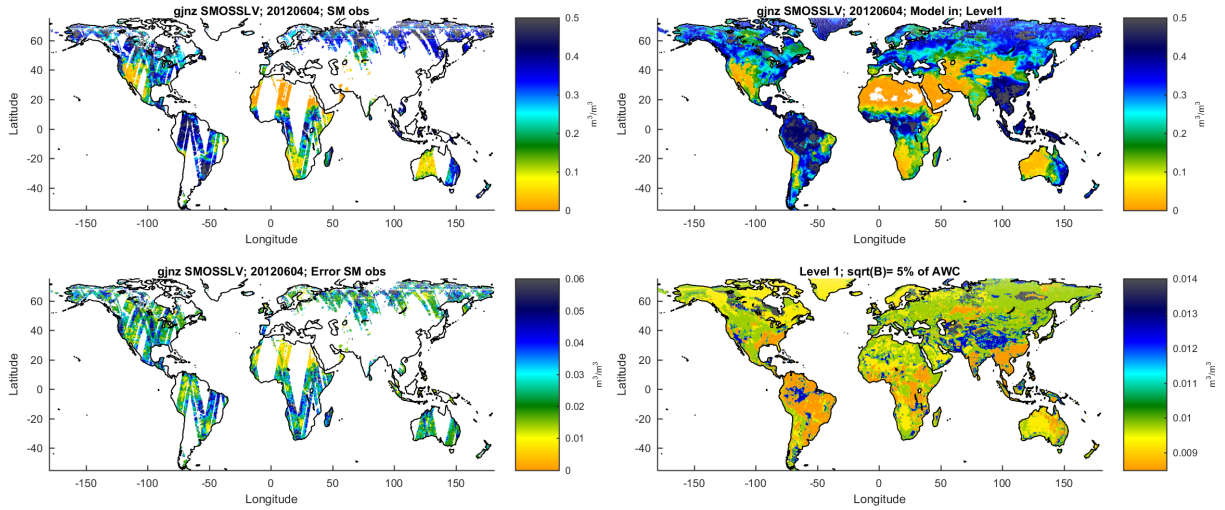

Figure 2: (Upper left:) SMOS NN SM for day 04 June 2012. (Lower left:) SMOS NN SM observation error taken as three times the NN output uncertainly in this example ($3 \times \sigma_{NN}$). (Upper right:) model background for the same day and first layer (SM_{L1}) (Lower right) Model background error (5% of the water holding capacity). Units are $m^3/m3$.

from local maximum and minimum T_b's and the associated SM values for the first layer of H-TESSEL (index I_2 in Rodríguez-Fernández et al. (2016)). However, in the context of this DA experiment, it seemed more pertinent not to add any information such as soil texture to the SMOS T_b's used as input to the NN to better understand the contribution of SMOS data to the assimilation. Therefore, the final configuration chosen was T_b's and soil moisture linear expectations for H and V polarizations and three angle bins from 30° to 45°. The training database was constructed using data from 10 November 2010 to 31 December 2013. The data were temporally sampled with a time step of 5 days (one day every five was kept for the training database). Finally, the data were also spatially sampled with a step of three grid points both in latitude and longitude (one ninth of the original EASE grid points were kept for the training). The reference SM dataset for the training phase was the ECMWF IFS soil moisture forecasts for the first layer (0-7 cm). IFS data were taken from SMOS auxiliary files where the ECMWF IFS data have been re-gridded from a Gaussian N400 grid to a EASE25 25 km Equal Area Scalable Earth (EASE-grid version 2) grid common of CATDS SMOS products using a bilinear spatial interpolation. In addition, ECMWF IFS data have been interpolated linearly in time to match the time of SMOS overpasses in between two consecutive 3 hours forecasts.

IFS snow depth and the temperature of the first soil layer were used to filter out regions with snow or frozen soils. The NN output uncertainty was computed taking into account the radiometric noise of the SMOS L3 T_b's and a 1% error for the reference SM as explained in Rodríguez-Fernández et al. (2016). The NN output was interpolated from the EASEv2 grid common to SMOS CATDS products to a reduced Gaussian grid N256, which is the Gaussian grid corresponding to the T511 spectral truncation.

2.5 In Situ Measurements and Evaluation Protocol

The analysed SM fields discussed in this study, along with the model open-loop, were evaluated against in situ measurements for a large number of sites. All of the in situ data were obtained from the International Soil Moisture Network (Dorigo et al., 2011). Since the microwave radiation detected from space comes from the first few centimeters of the soil, only SM measurements at the 0-5 cm depth range were used. The sites are located in four continents and cover a large spectrum of climate conditions. Table 1 shows a summary of the networks used with the depth of the measurement and the location. Figure 1 shows the position of most of

Table 2: Experiments compared in this study. Experiment labels are shown in column 1. Column 2 shows the SM dataset assimilated if any. Column 3 shows the observation error assumed for the SM dataset. σ_{NN} and σ_{ascat} are provided by the retrieval algorithms and are variable in space and time. Figure 2 shows an example of σ_{NN}. Column 4 shows if T_{2m} and RH_{2m} are also assimilated for each experiment.

Label	SM	σ_{SM}	SLV
OL	no	...	no
SMOS1	SMOS NN	$1 \times \sigma_{NN}$	no
SMOS3	SMOS NN	$3 \times \sigma_{NN}$	no
SMOS9	SMOS NN	$9 \times \sigma_{NN}$	no
SMOS1-SLV	SMOS NN	$1 \times \sigma_{NN}$	yes
SMOS3-SLV	SMOS NN	$3 \times \sigma_{NN}$	yes
SMOS9-SLV	SMOS NN	$9 \times \sigma_{NN}$	yes
ASCAT1	ASCAT	$1 \times \sigma_{ascat}$	no
ASCAT2	ASCAT	$2 \times \sigma_{ascat}$	no
ASCAT4	ASCAT	$4 \times \sigma_{ascat}$	no
ASCAT1-SLV	ASCAT	$1 \times \sigma_{ascat}$	yes
ASCAT2-SLV	ASCAT	$2 \times \sigma_{ascat}$	yes
ASCAT4-SLV	ASCAT	$4 \times \sigma_{ascat}$	yes

them.

3 Methods

3.1 Offline surface-only land data assimilation system

The data assimilation framework used in this study is the ECMWF surface-only Land Data Assimilation System (so-LDAS). The so-LDAS performs a SM analysis ingesting information contained in various observations; from analysed screen level parameters (T_{2m} and RH_{2m} provided by the IFS-LDAS) to satellite-derived surface soil moisture (e.g. from ASCAT or SMOS). The observation inputs must be provided in the same grid of the model. The so-LDAS relies on an offline sequential data assimilation in a 24-hours window, based on the H-TESSEL land surface model (Balsamo et al., 2009) with ERA-Interim atmospheric forcing (Dee et al., 2011). Table 3 summarizes the main differences of the so-LDAS and the LDAS of the Integrated Forecast System (IFS-LDAS). The so-LDAS analysis is based on the same point-wise Simplified Extended Kalman filter scheme as the IFS-LDAS (de Rosnay et al., 2013).

The control vector x has three elements corresponding to the soil moisture from the three first soil layers of the model. For each observation within the assimilation window, the observation vector y_o has one element when only remote sensing SM from SMOS or ASCAT is assimilated or three elements if T_{2m} and RH_{2m} are also assimilated. The observation operator, h, transforms the model control variables at time $t = 0$ (start of assimilation window) into the observation space at the observation time t. Thus, the model counterpart to the observation vector is:

$$y^t = h(x^0) \tag{4}$$

For each assimilation step, the difference of the model (first guess) and the observations is called the *first guess departure* or *innovation* and can be expressed as:

$$(y^t_o - h(x^0_f)) \tag{5}$$

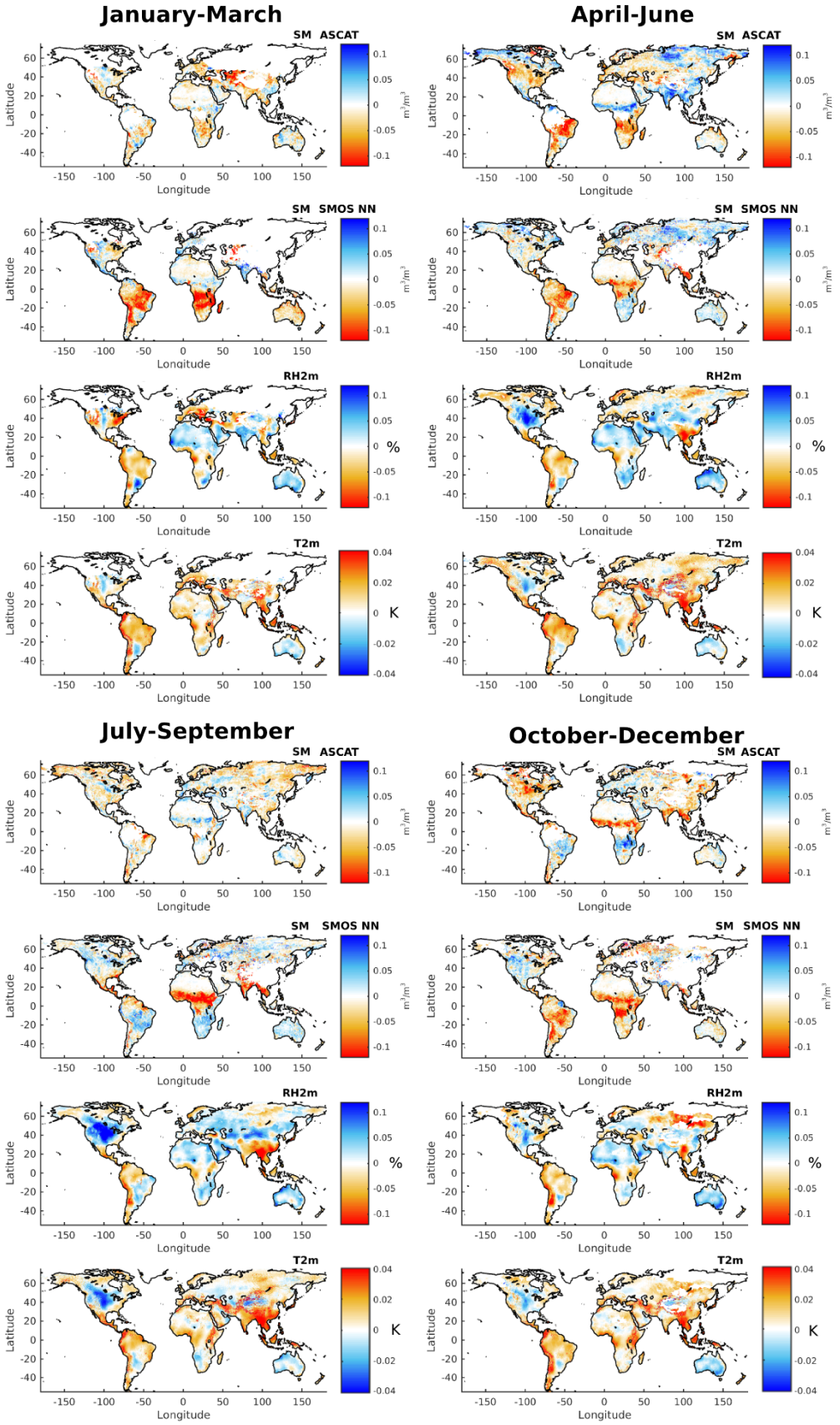

Figure 3: Mean innovations (Observation minus Model, Eq. 5) for periods of three months, expressed in m^3/m^3 for ASCAT and SMOS, in % for RH_{2m} and in K for T_{2m}.

Table 3: Comparison of the IFS Land Data Assimilation System (LDAS) and the surface-only LDAS

	IFS-LDAS	so-LDAS
Assimilation technique	SEKF	SEKF
Assimilation window	12 hours	24 hours
Surface-atmosphere coupling	fully coupled	uncoupled, surface forced by ERA-Interim
Observation input grid	Independent of the model grid	Same grid as the model grid
Analysis	RH_{2m}, T_{2m}, SM, soil temperature, snow cover and snow temperature	SM
Observation input	RH_{2m}, T_{2m}, ASCAT SM, LST, snow cover and snow temperature, SMOS TBs (in development)	RH_{2m} and T_{2m} analysed with IFS-LDAS, ASCAT SM, SMOS SM

The analysis increments, Δx, are the quantities used to correct the model after the assimilation of the observations. They are computed as the product of the *Kalman gain* matrix K and the innovation vector.

$$\Delta x = K(y_o^t - h(x_f^0)) \tag{6}$$

In the ECMWF implementation the Kalman gain is computed as:

$$K = BH^T(HBH^T + R)^{-1} \tag{7}$$

where B is the background error covariance matrix, R is the observation error covariance matrix and H is the Jacobian of the observation operator.
For instance, in the case of assimilating only SM, the Jacobian matrix is the vector:

$$H^t = \left(\frac{\partial SM^t}{\partial SM_{L1}^0} \frac{\partial SM^t}{\partial SM_{L2}^0} \frac{\partial SM^t}{\partial SM_{L3}^0} \right) \tag{8}$$

The elements of the Jacobian matrix are estimated by finite differences, by individually perturbing each component x_j of the control vector x by a small amount δx_j to get for each integration a column of the matrix H:

$$H_{ij} = \frac{y_i(x + \delta x_j) - y_i(x)}{\delta x_j} \tag{9}$$

The observations are assimilated over a 24 h window divided in 1-hour bins in the UTC reference frame. In the current version of the so-LDAS, only the T_{2m} and RH_{2m} observations from 3:00 to 21:00 UTC are taken into account. All the remote sensing (ASCAT or SMOS) measurements in the full 24 hours window are used. The increments are applied at the beginning of the 24-hour data assimilation window, as in the simplified 2D-VAR proposed by Balsamo et al. (2004). For every 24-hour analysis cycle, five trajectories of H-TESSEL are produced: (1) the first trajectory provides the model background, (2-3-4) three more trajectories are produced by perturbing the soil moisture initial condition of first, second and third layer, respectively, (5) in the last trajectory the analysis increments are applied at the beginning of the 24-hour window. It provides the analysed trajectory.

The background error covariance matrix B is assumed to be not dependent on time (simplified EKF). For each

grid point, B is a function of the errors σ of the three upper model layers:a

$$B \equiv \begin{pmatrix} \sigma_b^2 & 0 & 0 \\ 0 & \sigma_b^2 & 0 \\ 0 & 0 & \sigma_b^2 \end{pmatrix} \tag{10}$$

In this study the background errors have been fixed to 5% of the water holding capacity, which depends on each grid point on soil texture. Figure 2 shows a global map of the model background error σ_b.

For each grid point, the observation error covariance matrix R is :

$$R \equiv \begin{pmatrix} \sigma_{T_{2m}}^2 & 0 & 0 \\ 0 & \sigma_{RH_{2m}}^2 & 0 \\ 0 & 0 & \sigma_{SM}^2 \end{pmatrix} \tag{11}$$

where $\sigma_{T_{2m}}$ and $\sigma_{RH_{2m}}$ are set to 2K and to 4%, respectively. The uncertainty of the remote sensing SM datasets (σ_{NN} or σ_{ascat}) is variable in space and time and it could be a lower limit to the actual observation error. Therefore, in the context of this data assimilation study, σ_{NN} and σ_{ascat} have been multiplied by different factors to compute the SM observation error σ_{SM}. The assimilation results (Sect. 4) are discussed for several configurations of the observation errors (different R matrices). Table 2 summarizes the assimilation experiments conducted for this study. An Open-Loop (OL, H-TESSEL without assimilation) is compared to six DA experiments with SMOS NN SM (three configurations of the observation errors, with and without SLVs) and six DA experiments with ASCAT SM (three configurations of the observation errors, with and without SLVs). As discussed in Sect. 4 and 5, the experiments with large values of SM observation errors (SMOS9-SLV, for instance) are close to the SLV-alone case, because the relative weight of the SM data for the assimilation is very low. So, the corresponding experiment results are expected to be close to an experiment that would have used SLVs only.

Compared to the IFS-LDAS, the so-LDAS, is running offline. This makes it very affordable in computing time. The current offline so-LDAS analyses require three days (instead of 6 months for an IFS-LDAS) of wall-clock time to run a one-year DA experiment. Using the so-LDAS allowed to run the extensive number of SMOS and ASCAT data assimilation experiments presented in this paper. The so-LDAS analysed soil moisture fields were used to initialse forecast-only atmospheric forecasts, allowing to evaluate the impact of SMOS and ASCAT soil moisture DA on NWP as detailed in Sect. 3.3.

3.2 Soil moisture analysis evaluation against in situ measurements

The analysed fields and the model open loop have been evaluated against in situ measurements using the following protocol. Sites and times covered by snow and with frozen soil (first layer temperature lower than 274 K) have been filtered out. The in situ measurements were compared to the closest model grid point. To select a given in situ measurement, a time window of $\pm$30 min around the model time was used. Data from a given time are used to compute statistics metrics only if an SM value is available for all of the datasets, ensuring that all time series contain exactly the same number of points. A minimum lower limit of 200 points in a time series has been fixed to use the time series to compute the metrics. Table 1 shows the number of sensors that satisfied the previous criteria for each network, and the mean number of points per time series for those sensors. The metrics are computed sensor by sensor with respect to the closest grid point. Afterwards, the metrics are averaged to show a global estimate of the performances against each network. The results are shown in Sect. 5.1.

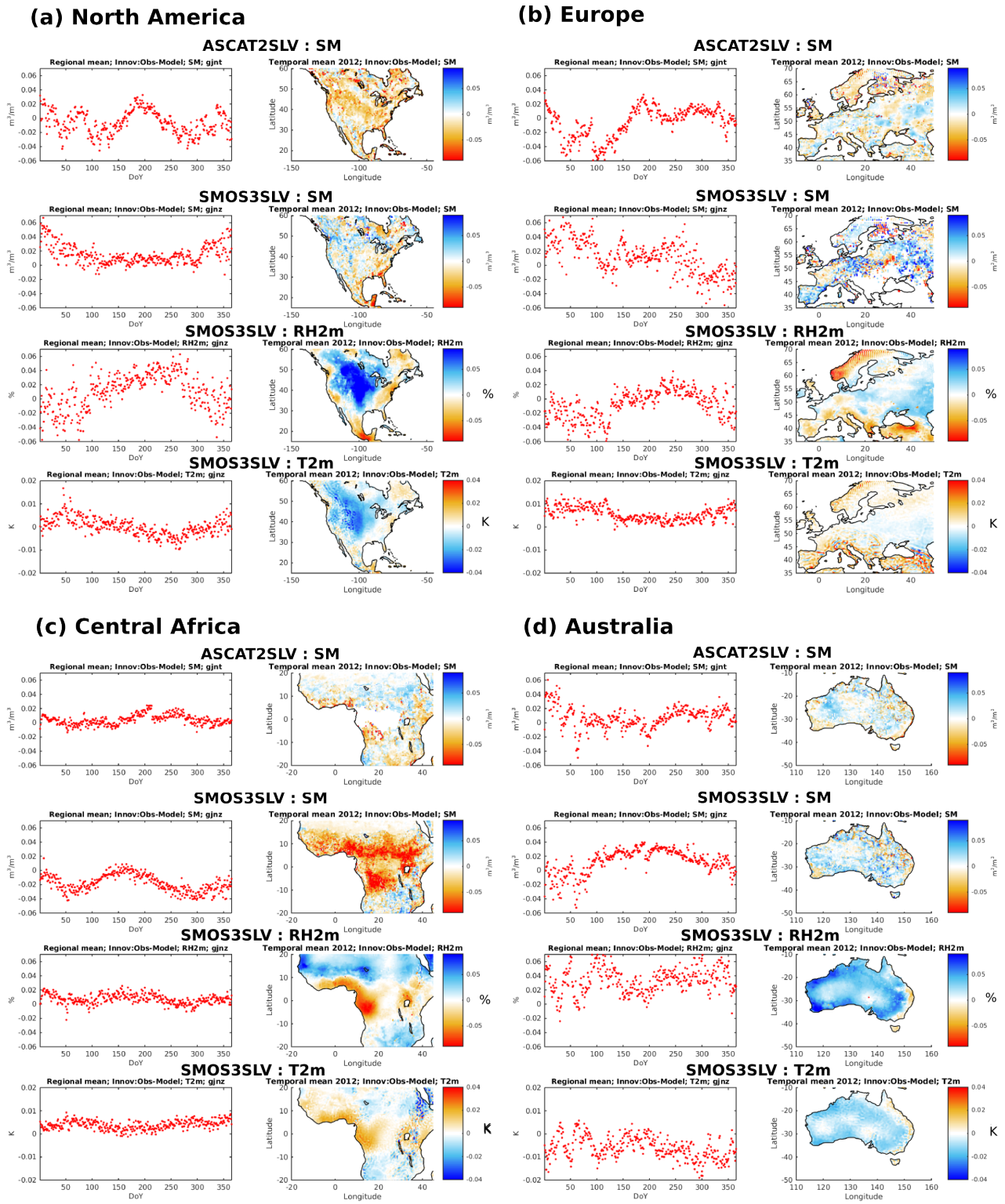

Figure 4: ***(a)*** *Left panels: time series of innovations averaged over the regions of North America shown in the right panels for the four observables: ASCAT SM and SMOS NN SM in m^3/m^3, T_{2m} in K, RH_{2m} in %). Right panels: maps of temporal averages of the innovations for the four observables over January-December 2012.* ***(b)*** *Same for Europe.* ***(c)*** *Same for central Africa.* ***(d)*** *Same for Australia.*

3.3 Impact of the soil moisture analysis on the forecast

The open-loop and the analysed surface fields were used to initialise atmospheric forecast experiments at a T511 resolution for the whole 2012. To evaluate the different forecasts, the following method was used. The analysis of the IFS that was operational in 2012 was used as reference (*truth*). The different forecasts were compared to this reference in periods of three months using several metrics as the root mean square difference (RMS) or the standard deviation (STD). In a second step, the scores obtained for the forecast using the surface model with no assimilation were subtracted to the scores obtained for the forecasts using analysed surface fields. Therefore, negative values imply that the forecast using analysed SM are closer to the *truth* than the forecast with no surface assimilation. The results are discussed in Sect. 5.2. Each 1-year forecast experiment using the output of the so-LDAS analyses takes in between three and four weeks of computing time in the current system. It is worth noting that the evaluation statistics are very robust as the forecast period is long and allows a detailed analysis for the different seasons.

4 Results

4.1 Innovations and Kalman gains

Figure 3 shows the mean innovations (Eq. 5) for ASCAT SM, SMOS SM, RH_{2m}, and T_{2m}, for January-March (JFM), April-June (AMJ), July-September (JAS) and October-December (OND). In general, the innovations for the different observables are in good agreement as they show similar geographical patterns. The sign of the innovations for T_{2m} are opposite that of the other observables, as expected, because the opposite relationship between T_{2m} and SM (*e.g.* in principle the more SM the lower T_{2m}, and conversely). However, some differences can be noticed for instance in the Sahel region: in AMJ and JAS ASCAT SM innovations are negative while those for SMOS SM, RH_{2m} and T_{2m} are in good agreement (positive for SMOS SM and RH_{2m} and negative for T_{2m}). Some differences are also observed in North America at all seasons: ASCAT SM innovations are negative all over the region while those of the other observables show different signs in the west and east coasts with respect to the central region. Other differences can be found in India, where innovations for different observables do not always have the same sign and in the Cambodian peninsula where innovations are always negative except for ASCAT in April-June. All innovations are in general good agreement in South America.

The innovations due to the four observables used in this study have been analysed further in four regions: North America, Europe, central Africa and Australia. Figure 4 shows temporal series of the innovations averaged over those regions and maps of temporal averages in the same regions. The time series of the spatial average of the innovations show some seasonal patterns for instance for ASCAT SM in North America and for SMOS NN SM in central Africa. In addition, there are some significant differences in the spatial patterns of the temporal averages of different observables. For instance:

- Innovations in North America for RH_{2m} are positive in most of the region (and negative for T_{2m}) while they are negative for ASCAT SM.
- The spatial extend of SMOS NN SM negative innovations in the Sahel region is larger than those obtained for RH_{2m} (they are more similar to the extension of positive innovations for T_{2m}).
- Over Australia, innovations for RH_{2m} are positive except in the East coast. Innovations for T_{2m} are in good agreement (with opposite sign as expected). In contrast, innovations for SM (both ASCAT and SMOS) are negative over significant regions in the centre and in the West coast.

Figure 5 shows the Kalman gains for the three first soil layers of the model when assimilating ASCAT SM (ASCAT2-SLV), SMOS SM, RH_{2m}, T_{2m} (SMOS3-SLV). Independently of the actual values, which depend on the observation error, gains for SMOS and ASCAT (Figs. 5**a,b**) show an overall good agreement for the three layers. For instance, for the first layers gains are high in Northern and Southern Africa, in Australia, North America, the Middle East and the South-East of South America. However, some differences can be noticed. Kalman gains for ASCAT SM decrease in Alaska and North Canada with respect to the values in lower latitudes of North America. In contrast, the Kalman gains for SMOS NN SM remain high. Gains for the second model layers are higher for SMOS NN SM than for ASCAT SM, in particular at high latitudes. Finally, gains for the third model layers are similar for SMOS NN SM and ASCAT SM. They become negative in both cases and they are only significant in the Equatorial region. The gains for SLV assimilation (Figs. 5**c,d**) are high in central Asia, Europe and the center and western part of North America. This distribution of high gains is complementary to those obtained for the assimilation of surface SM (Figs. 5**a,b**).

4.2 Increments: SMOS NN SM and ASCAT SM

Figures 6**a-c** show the sum of the increments in the period from July to September as a function of the observation error. As expected, when the observation errors increase the increments decrease from values larger than 10 mm (SMOS1) to to $\sim$ 10 mm (SMOS3) and lower than $\sim$ 5 mm (SMOS9) for the first model layer. For the first model layer, the increments show clear geographical patterns, being negative in the Sahel region and from the north of South America to the south of North-America and positive elsewhere. The increments in the second model layer are smaller but still significant close to the Equator and at high northern latitudes. Finally, Fig. 6c shows that when the observation error is very high (SMOS9), SMOS NN SM data are almost not assimilated.

The seasonal behaviour of the assimilation of SMOS NN SM is shown in Fig. 7. Cumulative increments in Australia, South Africa and parts of South America are negative in January-March and October-December and they are positive from April to September. Interestingly, the seasonal analysis of the increments obtained when assimilating ASCAT SM also show seasonal patterns in those regions (Fig. 8). However, there is a kind of three months lag with respect to the assimilation of SMOS NN SM as cumulative increments in Australia, South Africa and parts of South America are mainly negative from January to June and positive from July to December. In addition, it is noteworthy that increments in July-September are positive in the Sahel when assimilating ASCAT SM (Fig. 8) while they are negative when assimilating SMOS NN SM (Fig. 7).

The increments have been analysed further in four regions: North America, Europe, central Africa and Australia. Left panels of Figs. 9**a-d** show temporal series of the increments averaged over those regions and maps of temporal averages in the same regions for the whole 2012. The time series of the spatial average of the increments for the first model layer show some seasonal patterns in central Africa and Australia. In Africa, the spatial average of the increments for the second model layer also shows a temporal pattern.

4.3 Increments: SM and SLV

This section discusses the assimilation of SLVs (T_{2m} and RH_{2m}). Experiments of assimilation of SLVs alone have not been run in the framework of this study. Nevertheless, it is possible to investigate the role of SLVs alone using the experiments for which the weight of surface SM observations is low (high observation errors). Figure 10 shows the sum of the absolute increments in the period July-September when assimilating SMOS SM NN or ASCAT SM with and without T_{2m} and RH_{2m}. The experiments shown in this figure have been chosen with high observations errors for SM (SMOS9 and ASCAT4) in order to give low weight to the remote sensed SM and to better show the effect of the assimilation of SLVs. Comparing Figs. 10**c,d** with Figs. **a,b**

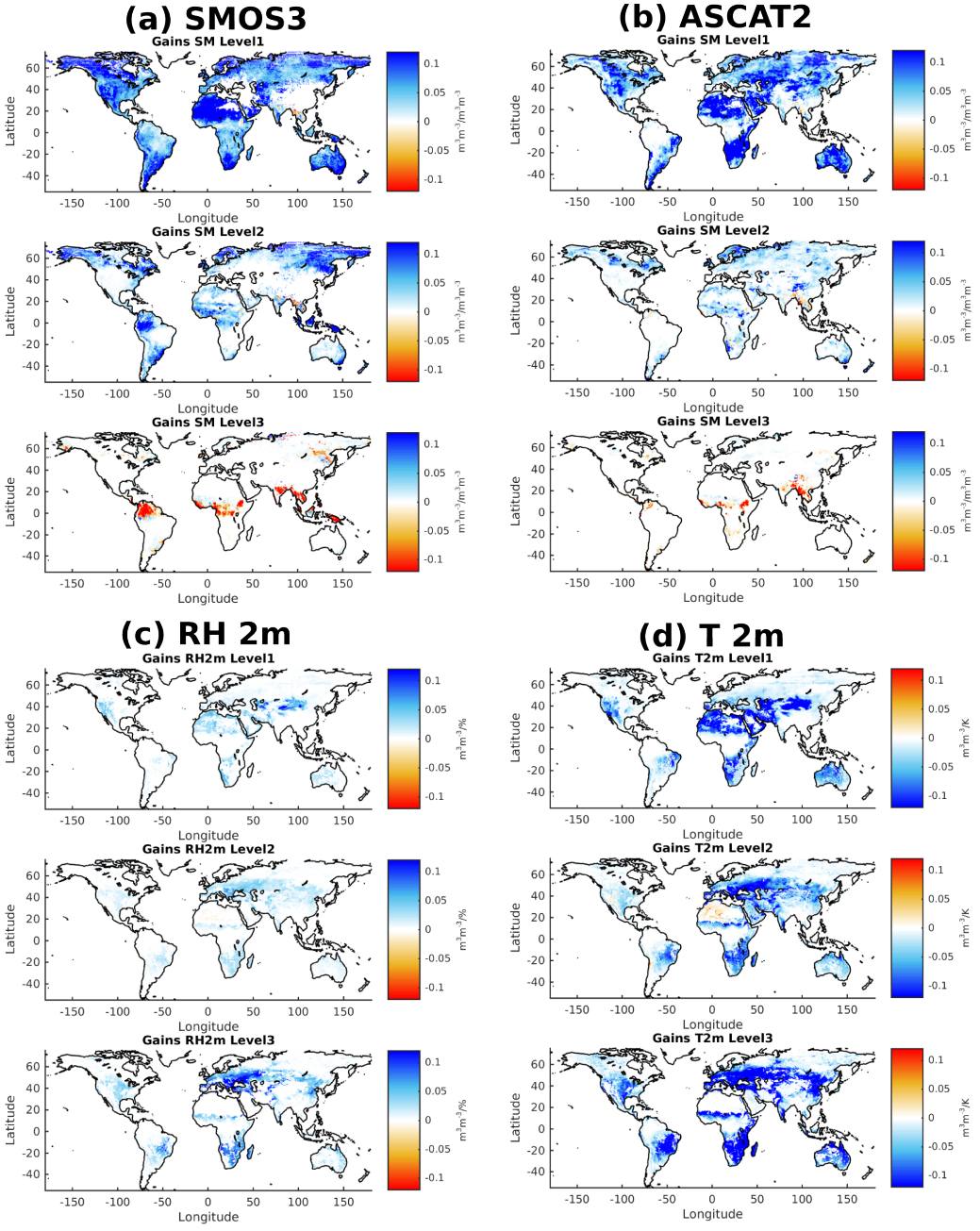

Figure 5: Mean Kalman gains for JAS for the first three model layers with respect to:) ***(a)*** *SMOS NN SM (experiment SMOS3-SLV),* ***(b)*** *ASCAT SM (experiment ASCAT2-SLV),* ***(c)*** RH_{2m} *(experiment SMOS3-SLV),* ***(d)*** T_{2m} *(experiment SMOS3-SLV). The Kalman gain is expressed in* $(m^3/m^3)/(m^3/m^3)$ *for (a) and (b); it is expressed in* $\%/(m^3/m^3)$ *for (c) and in* $K/(m^3/m^3)$ *in (d).*

.

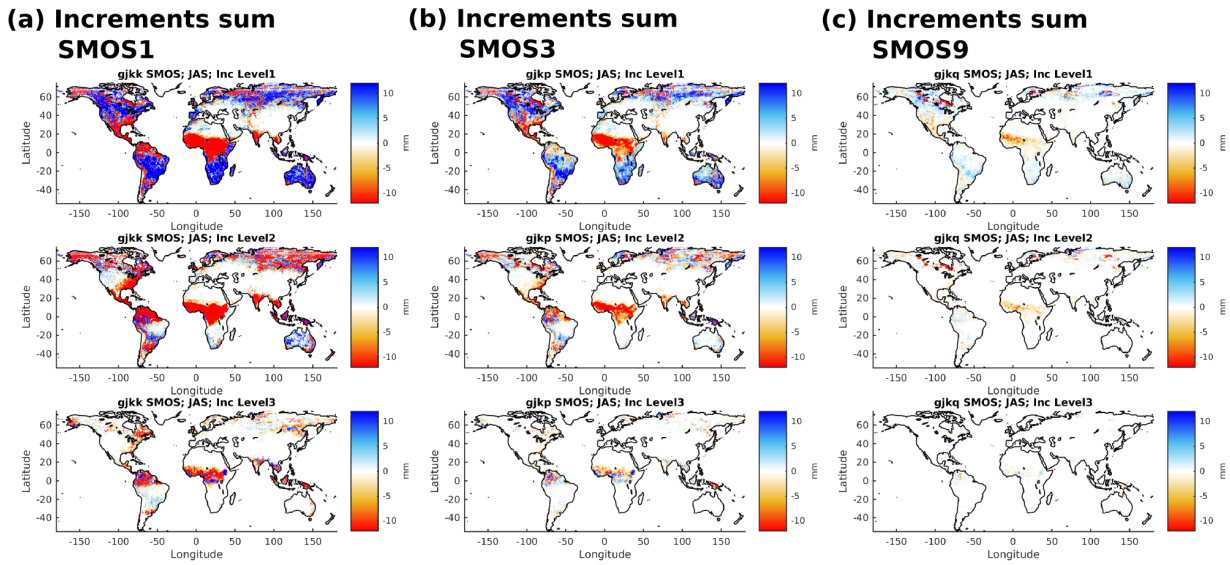

Figure 6: Increments sum in mm for the period July-September for experiments SMOS1, SMOS3 and SMOS9 (panels a to c, respectively).

it is possible to see that the increments in the first layer due to the assimilation of SLVs are significant in the west of North America, central Asia, the Sahel and South Africa, part of the Amazon region, and Australia. In contrast to the remote sensing measurements of surface SM, the SLVs contain significant information on the SM content at deeper soil layers. Figures 10**c,d** show that the cumulative increments for layers 2 and 3 are still relatively large at depth, with basically the same spatial patterns than in layer 1.

The results of two experiments that assimilate SLVs together with surface SM from SMOS NN or ASCAT are shown in Figs. 11 (SMOS3+SLV) and 12 (ASCAT2+SLV), respectively. The most significant difference comparing ASCAT2 (Fig. 8) and ASCAT2+SLV (Fig. 12) was found in July-September. The cumulative increments in parts of North America, central Asia and Australia are positive for ASCAT2+SLV while they are negative or close to zero for ASCAT2 (Fig. 8). The increments obtained when assimilating SMOS NN SM alone (Fig. 7) or with SLV (Fig. 11) are in general good agreement. It is noteworthy that the analysis of SLV give positive increments in Asia in zones were SMOS data is not available due to contamination by artificial emission at 1.4 GHz (radio frequency interference, RFI).

5 Discussion

5.1 Evaluation of the soil moisture analysis

The analysed soil moisture fields and the model open loop were compared to in situ measurements of soil moisture for the sites discussed in Sect. 2 using the protocol presented in Sect. 3.2. Figure 13 shows an example of the time series obtained for one site of the SCAN network in North America. The analysed SM time series become closer to the open loop as the observation error increases (SMOS3, SMOS3+SLV, SMOS9+SLV). For this network, times series with and without assimilation of SLV (for the same SM error) are very similar. In this particular case, the assimilation of SMOS SM with a low error (SMOS1) improves significantly the match with the in situ measurements in June-July and in October-December. In the case of the assimilation of ASCAT SM (the two lower panels), the open loop and the analysed time series are very close.

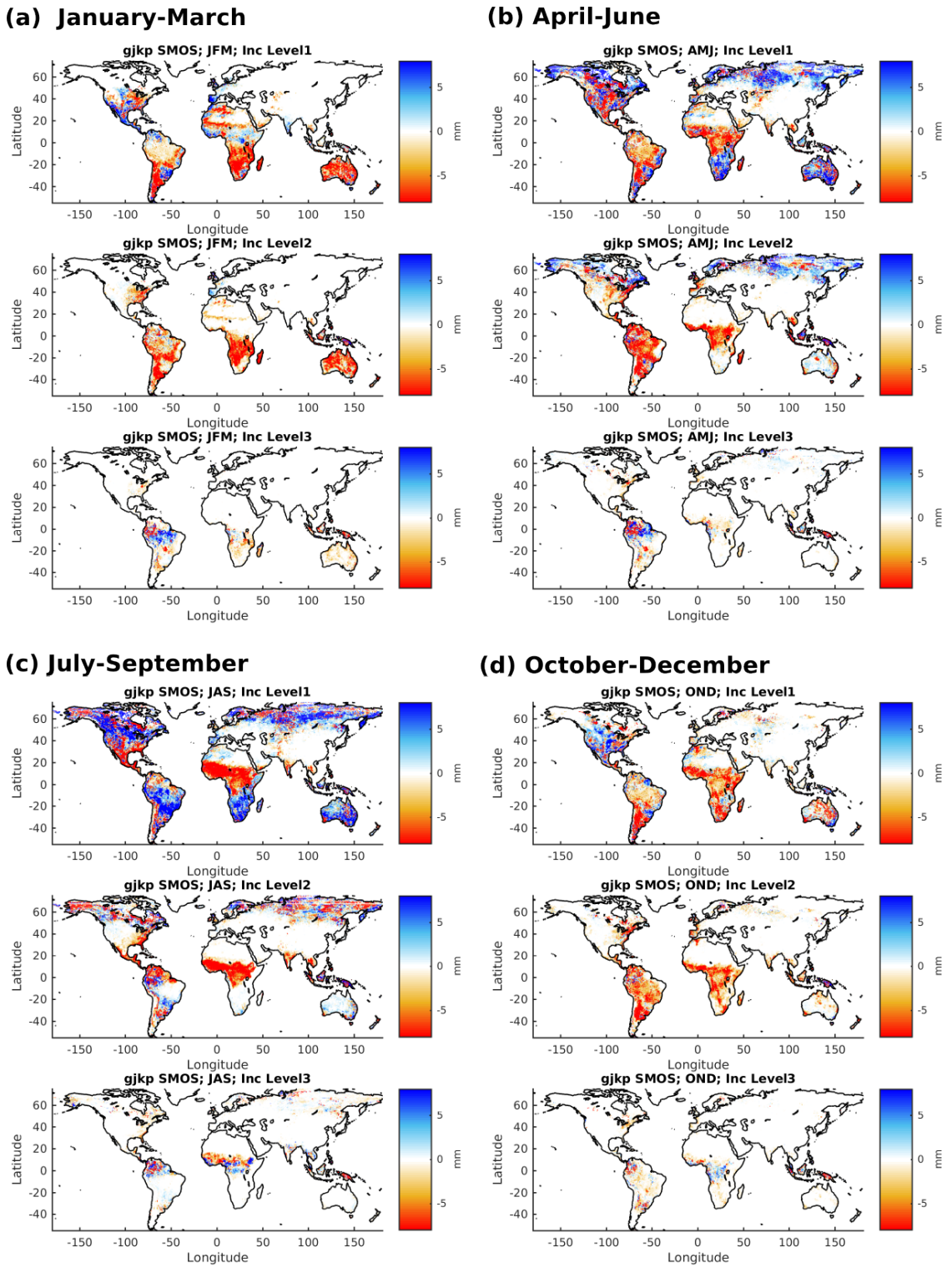

Figure 7: Increments for the first three model layers for experiment SMOS3. ***(a)*** *Sum of the increments from January to March.* ***(b)*** *Sum of the increments from April to June.* ***(c)*** *Sum of the increments from July to September.* ***(d)*** *Sum of the increments from October to December.*

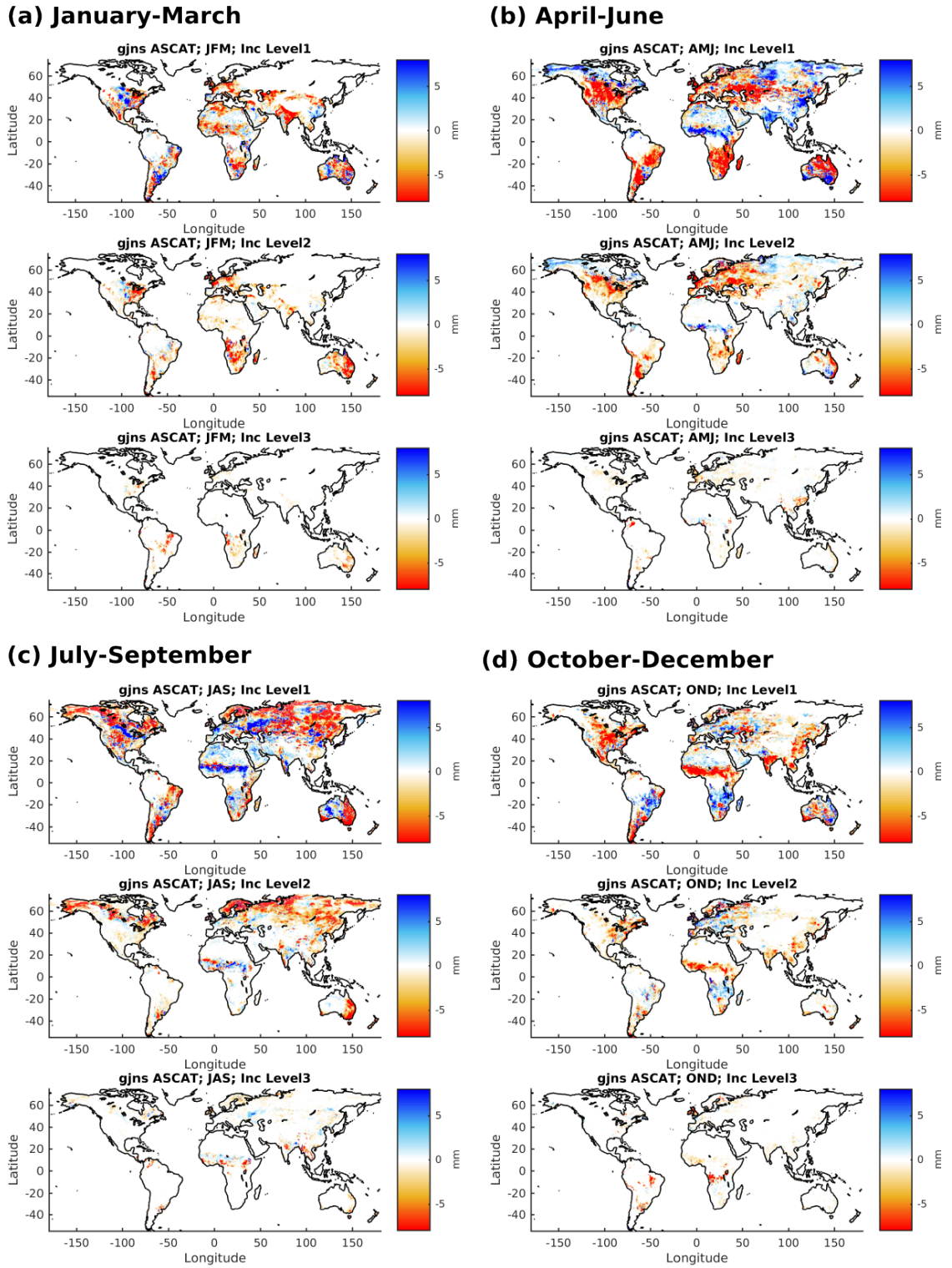

Figure 8: Increments for the first three model layers for experiment ASCAT2. ***(a)*** *Sum of the increments from January to March.* ***(b)*** *Sum of the increments from April to June.* ***(c)*** *Sum of the increments from July to September.* ***(d)*** *Sum of the increments from October to December.*

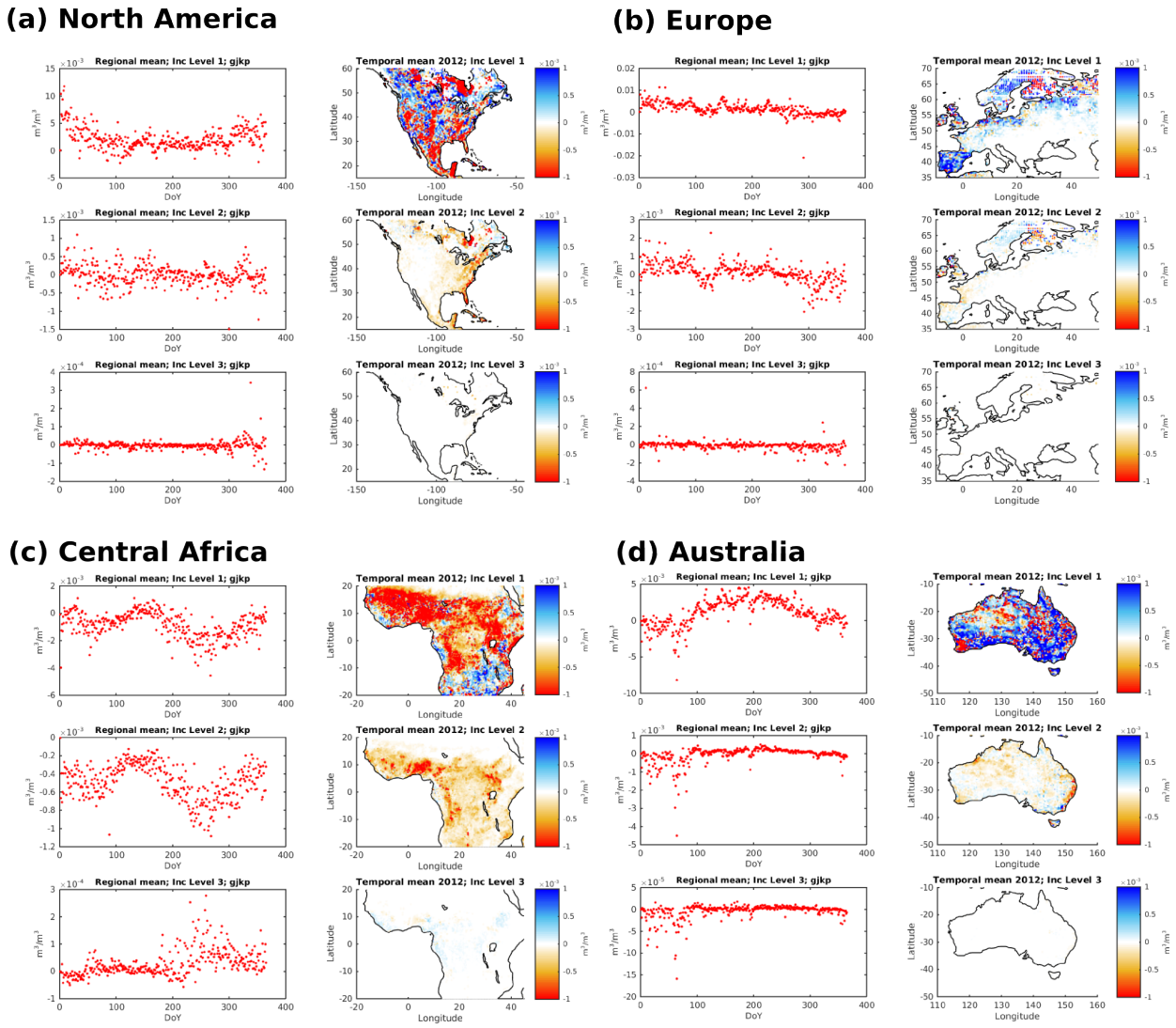

Figure 9: Increments for experiment SMOS3. ***(a)*** *Left panels: time series of increments averaged over the regions of North America shown in the right panels for the three upper model layers. Right panels: maps of temporal averages of the innovations for the three model layers over January-December 2012.* ***(b)*** *Same for Europe.* ***(c)*** *Same for central Africa.* ***(d)*** *Same for Australia.*

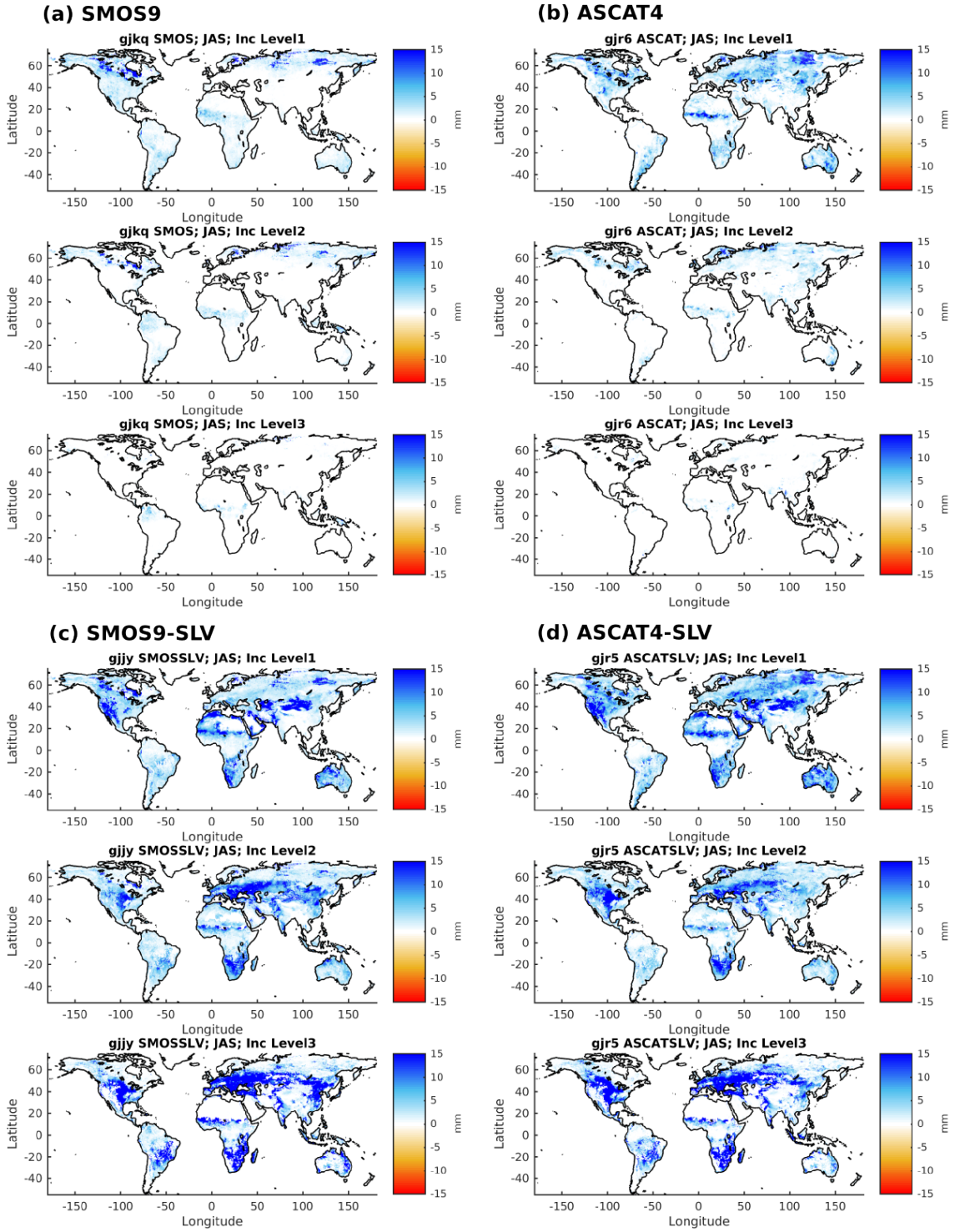

Figure 10: Sum of absolute soil moisture increments (in mm) for the period July-September for the three upper model layers for experiments: (a) SMOS9, (b) ASCAT4, (c) SMOS9-SLV and (d) ASCAT4-SLV.

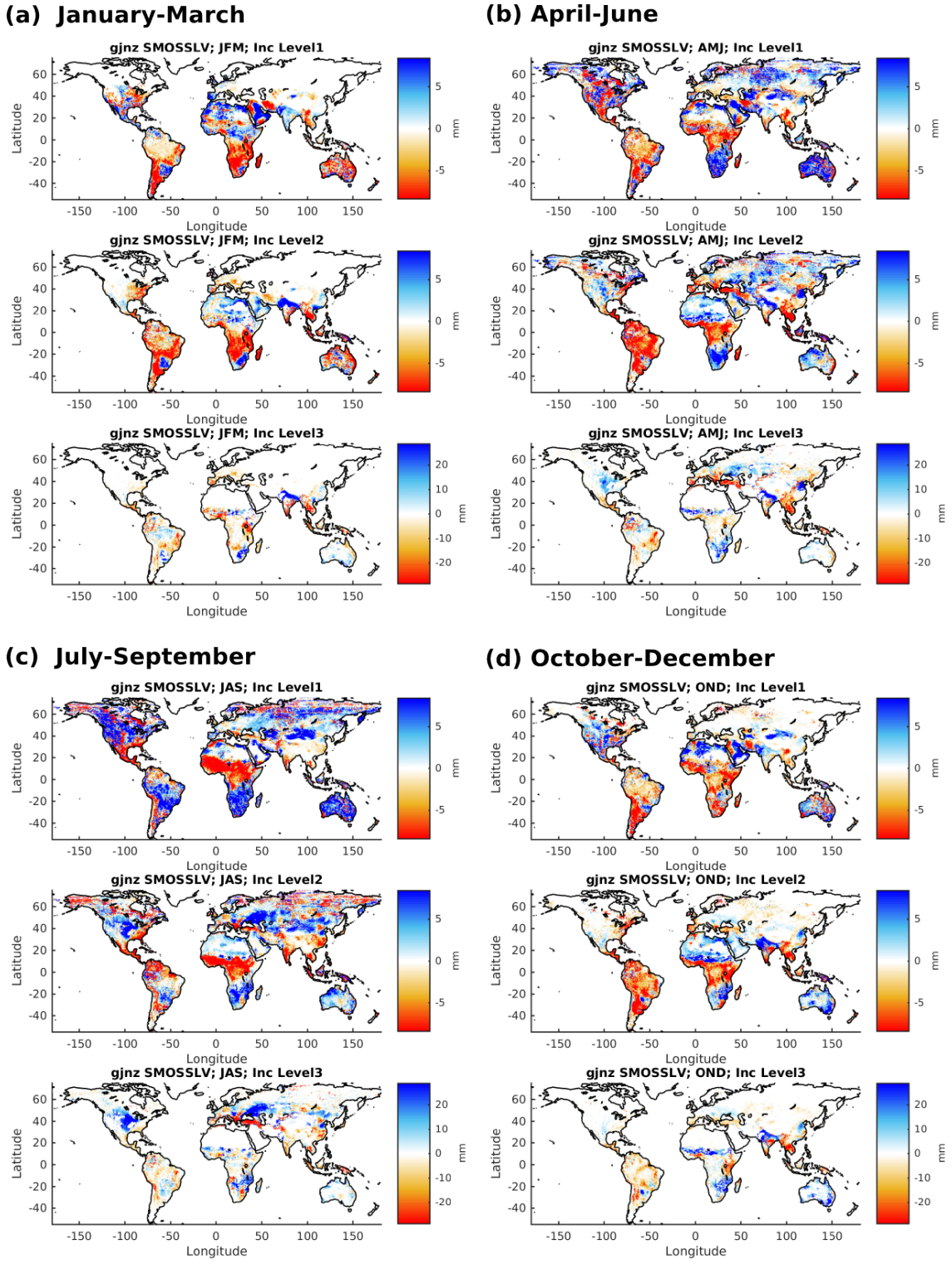

Figure 11: Soil moisture increments, in mm, for the first three model layers for experiment SMOS3+SLV, accumulated for ***(a)*** *January to March.* ***(b)*** *April to June.* ***(c)*** *July to September.* ***(d)*** *October to December.*

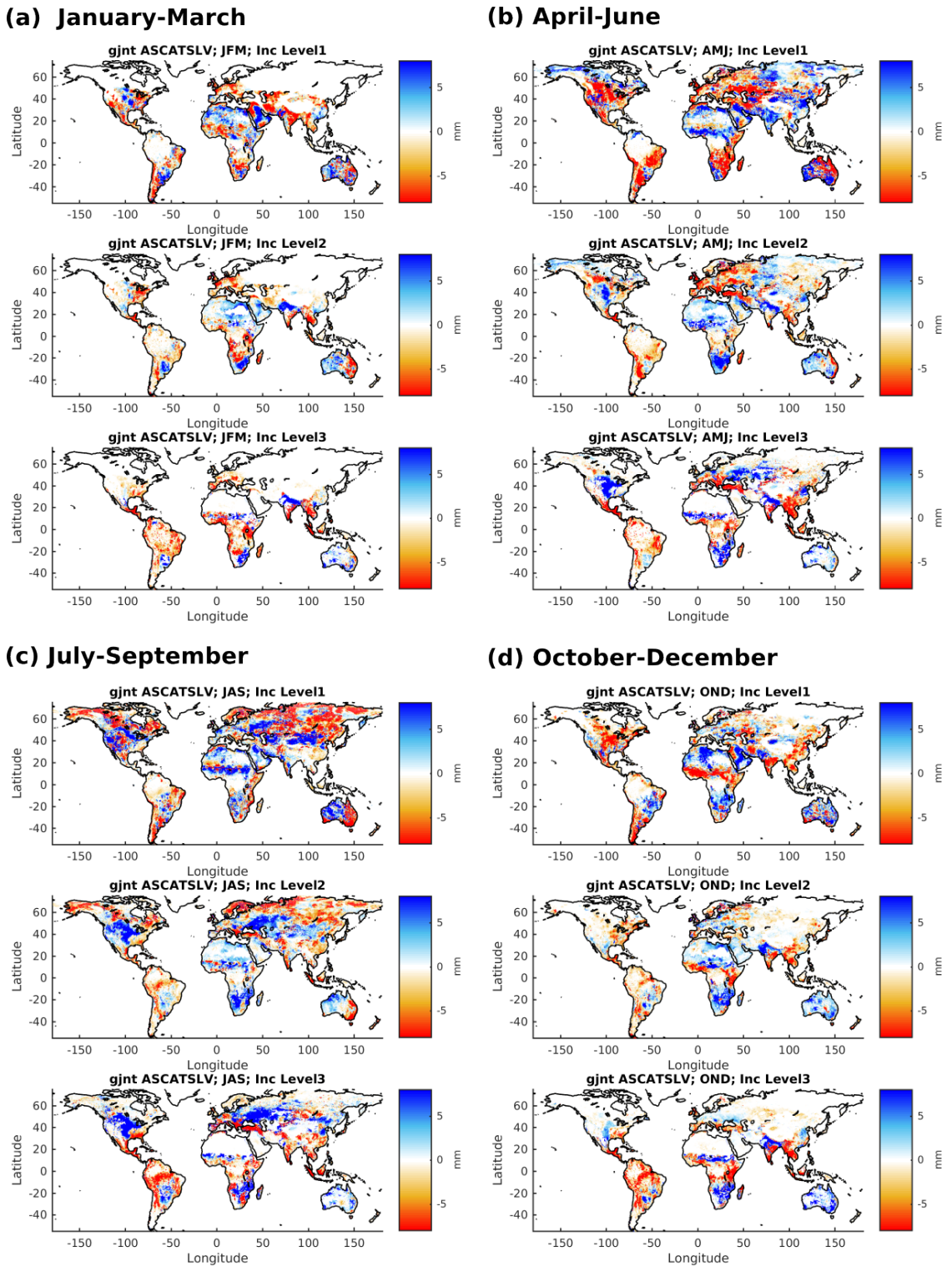

*Figure 12: Soil moisture increments, in mm, for the first three model layers for experiment ASCAT2+SLV, accumulated for **(a)** January to March. **(b)** April to June. **(c)** July to September. **(d)** October to December.*

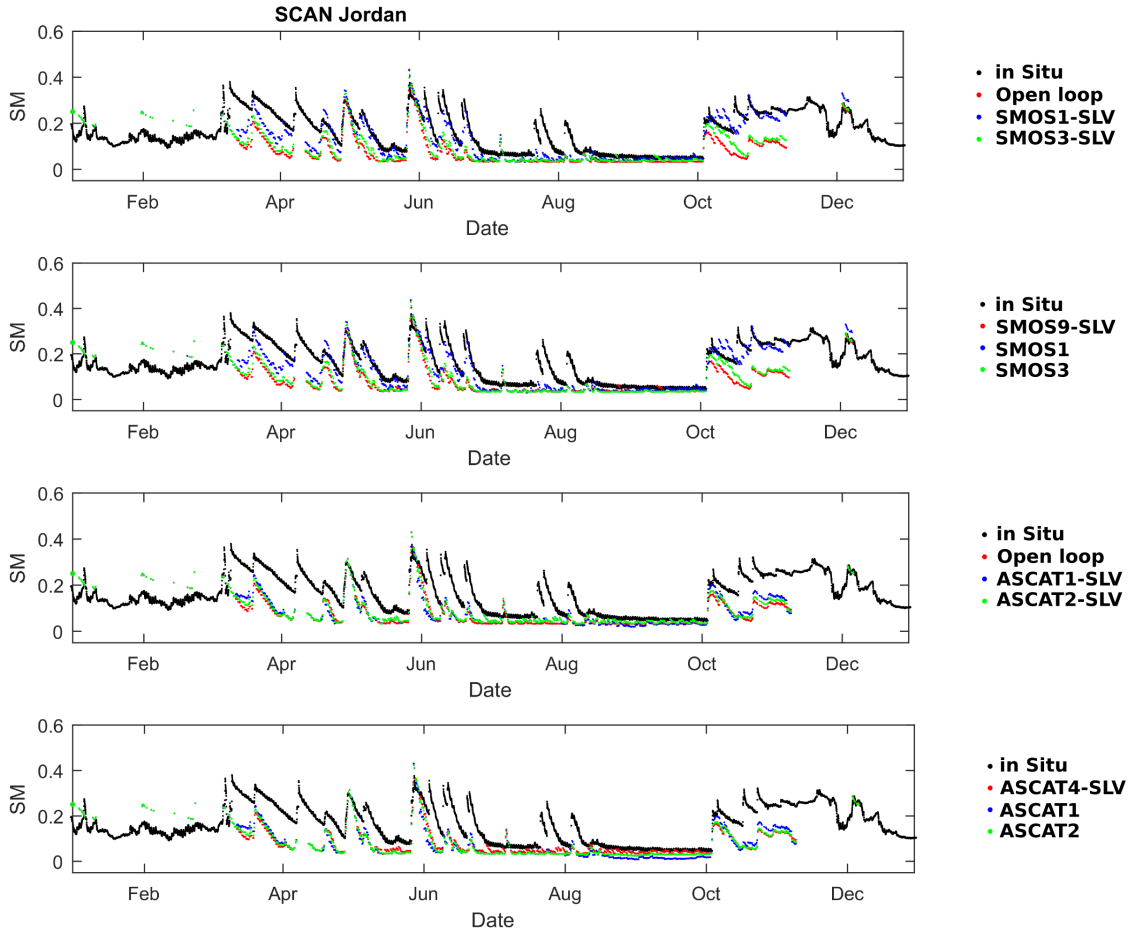

Figure 13: Time series for 2012, at the SCAN Jordan station, of soil moisture ($m^3.m^3$) in situ measurements (black dots), model open loop and to surface analyses obtained by assimilation of SMOS or ASCAT with different observation errors, with and without SLV (see Table 2 for an explanation of the experiment labels).

In order to get more general results, different statistical metrics have been computed site per site and the values have been averaged per network. Table 4 shows the results. Three different cases were identified:

1. *Scores improve when the SM datasets are assimilated with a low observation error.* For instance, in the case of ARM, the metrics improve when SMOS NN SM is assimilated with a low error (SMOS1, SMOS1+SLV). For instance the Pearson correlation goes from 0.64 to 0.63 and 0.61 for SMOS1 to SMOS9. In all cases, the analysed fields give better results than the open loop. A similar behaviour has been found with the assimilation of ASCAT in the chinese network CTP-SMTMN (better results for ASCAT1 than for ASCAT2 or ASCAT4).

2. *Scores improve when the SM datasets are assimilated with a higher observation error.* In the case of FMI, DAHRA, HOBE or SNOTEL, the agreement with in situ measurements improves when the SM observation error increases, both for SMOS and ASCAT (with and without SLVs). In the case of FMI, only experiments with the highest observation errors (SMOS9 and ASCAT4, with and without SLVs) show scores comparable to the open loop. For the other sites, the experiments with the intermediate observation weight SMOS3, ASCAT2 (and their contourparts with SLVs) also give results similar to those obtained for the open loop.

3. *Scores of the SM analysis and the open loop are similar.* For networks such as SCAN, SMOSMANIA or PERUGIA the different analysis and the open loop give the same statistics independently of the observation error.

In conclusion, even if there are significant differences for some sites (Fig. 13), on average, the SM analysis gives similar results to the open loop. The effect of the observation error is different for different networks of in situ measurements but it has a relatively low impact overall. One must bear in mind that the ratio of observation error versus model error is in principle different for each site and it can be high in some places, giving low weight to the observations for the DA. It is also important to remark that the regions with more SM in situ measurements (North America and Europe) are also those were NWP models are the best constrained by a large number of conventional observations. Finally, even if the SM evaluation has been done in a large number of sites, it is, of course, not representative of the entire globe.

5.2 Sensitivity of the atmosphere to the soil moisture analysis

As explained in Sect. 3.3, the open-loop and the analysed surface fields were used to compute atmospheric forecast experiments for the whole year 2012, which were evaluated with respect to the IFS analysis in periods of three months using several metrics as the root mean square difference (RMS) or the standard deviation (STD). The metrics obtained for the forecast using as input the SM analysis were compared to those of the forecast with no assimilation. Some of the results are shown in Figs. 14 - 16 as the difference in RMS of the DA experiments minus the forecast using the open loop. Negative scores imply that the RMS of the DA experiments with respect to the IFS analysis are lower than those of the open loop. Therefore, negative scores mean that the forecast using the analysed surface fields is better than using the open loop.

Figure 14 shows the skill to forecast T_{2m} as a function of the forecast day averaged in periods of three months for the experiments using SMOS NN SM. The results were computed for the Southern Hemisphere, the tropical region and the Northern Hemisphere. Figure 15 shows the equivalent results but for the experiments using ASCAT SM.

The sections below comment on the results of the forecast for T_{2m}. Similar results were found for RH_{2m} or for the dew point forecast.

Table 4: Evaluation against in situ measurements. Mean standard deviation (STD), Pearson correlation (R) and bias with respect to the in situ measurements for each network of in situ sensors.

SM	Mean STD	Mean R	Mean Bias	Mean STD	Mean R	Mean Bias	Mean STD	Mean R	Mean Bias
	ARM Sensors= 31; Npt= 717			HOBE Sensors= 46; Npt= 687			SCAN Sensors= 240; Npt= 816		
SMOS1	0.058	0.64	0.040	0.037	0.68	-0.002	0.054	0.54	0.043
SMOS3	0.061	0.63	0.034	0.038	0.71	-0.010	0.055	0.55	0.038
SMOS9	0.064	0.61	0.030	0.039	0.71	-0.013	0.056	0.54	0.036
SMOS1-SLV	0.058	0.64	0.040	0.037	0.68	-0.002	0.054	0.54	0.043
SMOS3-SLV	0.060	0.63	0.035	0.038	0.71	-0.009	0.055	0.55	0.038
SMOS9-SLV	0.064	0.60	0.031	0.038	0.71	-0.012	0.056	0.54	0.036
ASCAT1	0.064	0.63	0.029	0.043	0.67	-0.016	0.056	0.54	0.032
ASCAT2	0.063	0.62	0.030	0.040	0.70	-0.015	0.055	0.54	0.034
ASCAT4	0.064	0.61	0.029	0.039	0.71	-0.014	0.056	0.54	0.035
ASCAT1-SLV	0.063	0.62	0.031	0.043	0.66	-0.016	0.056	0.53	0.033
ASCAT2-SLV	0.063	0.61	0.031	0.040	0.70	-0.014	0.055	0.54	0.035
ASCAT4-SLV	0.064	0.60	0.031	0.039	0.71	-0.013	0.056	0.54	0.035
OL	0.065	0.60	0.029	0.039	0.71	-0.014	0.056	0.54	0.035
	CTP-SMTMN Sensors= 33; Npt= 365			PERUGIA Sensors= 2; Npt= 719			SMOSMANIA Sensors= 19; Npt= 1009		
SMOS1	0.048	0.53	0.114	0.057	0.79	0.078	0.053	0.79	0.066
SMOS3	0.048	0.53	0.114	0.057	0.79	0.079	0.053	0.80	0.063
SMOS9	0.048	0.53	0.114	0.057	0.79	0.079	0.054	0.80	0.062
SMOS1-SLV	0.048	0.53	0.113	0.057	0.79	0.074	0.053	0.79	0.065
SMOS3-SLV	0.048	0.53	0.113	0.057	0.79	0.075	0.053	0.80	0.062
SMOS9-SLV	0.048	0.53	0.113	0.057	0.79	0.075	0.053	0.80	0.060
ASCAT1	0.047	0.57	0.113	0.056	0.78	0.067	0.054	0.79	0.059
ASCAT2	0.048	0.54	0.114	0.057	0.79	0.075	0.053	0.80	0.060
ASCAT4	0.048	0.53	0.114	0.057	0.79	0.078	0.054	0.80	0.061
ASCAT1-SLV	0.047	0.57	0.113	0.056	0.78	0.064	0.054	0.79	0.059
ASCAT2-SLV	0.047	0.55	0.113	0.057	0.79	0.072	0.053	0.80	0.060
ASCAT4-SLV	0.048	0.54	0.113	0.057	0.79	0.075	0.053	0.80	0.060
OL	0.048	0.53	0.114	0.057	0.79	0.079	0.054	0.80	0.062
	DAHRA Sensors= 1; Npt= 1137			PBO-H2O Sensors= 101; Npt= 206			SNOTEL Sensors= 347; Npt= 537		
SMOS1	0.044	0.68	0.109	0.047	0.62	0.045	0.076	0.42	0.050
SMOS3	0.048	0.71	0.112	0.047	0.63	0.038	0.074	0.47	0.037
SMOS9	0.052	0.71	0.116	0.048	0.62	0.036	0.074	0.48	0.033
SMOS1-SLV	0.046	0.68	0.111	0.047	0.62	0.046	0.076	0.42	0.050
SMOS3-SLV	0.050	0.72	0.115	0.047	0.63	0.040	0.074	0.46	0.038
SMOS9-SLV	0.054	0.72	0.118	0.047	0.62	0.038	0.074	0.48	0.035
ASCAT1	0.059	0.71	0.097	0.047	0.63	0.031	0.076	0.45	0.025
ASCAT2	0.057	0.73	0.098	0.047	0.63	0.033	0.074	0.47	0.029
ASCAT4	0.057	0.74	0.102	0.048	0.62	0.034	0.074	0.48	0.031
ASCAT1-SLV	0.059	0.71	0.098	0.047	0.62	0.033	0.076	0.45	0.027
ASCAT2-SLV	0.058	0.73	0.099	0.047	0.62	0.035	0.075	0.47	0.032
ASCAT4-SLV	0.058	0.75	0.103	0.047	0.62	0.037	0.074	0.47	0.034
OL	0.053	0.72	0.117	0.048	0.62	0.036	0.074	0.48	0.032
	FMI Sensors= 8; Npt= 245			REMEDHUS Sensors= 23; Npt= 1016			USCRN Sensors= 122; Npt= 931		
SMOS1	0.030	0.49	0.114	0.065	0.79	0.114	0.053	0.66	0.081
SMOS3	0.026	0.36	0.134	0.064	0.80	0.115	0.052	0.68	0.076
SMOS9	0.023	0.59	0.109	0.064	0.79	0.115	0.053	0.67	0.073
SMOS1-SLV	0.031	0.41	0.116	0.065	0.79	0.113	0.053	0.66	0.082
SMOS3-SLV	0.026	0.36	0.134	0.064	0.80	0.113	0.052	0.68	0.076
SMOS9-SLV	0.023	0.59	0.109	0.064	0.80	0.112	0.053	0.67	0.074
ASCAT1	0.023	0.54	0.128	0.065	0.78	0.110	0.053	0.67	0.068
ASCAT2	0.023	0.58	0.115	0.064	0.79	0.113	0.052	0.68	0.071
ASCAT4	0.024	0.60	0.107	0.064	0.79	0.115	0.053	0.68	0.072
ASCAT1-SLV	0.023	0.54	0.128	0.065	0.78	0.110	0.052	0.67	0.069
ASCAT2-SLV	0.023	0.57	0.115	0.064	0.80	0.112	0.052	0.68	0.072
ASCAT4-SLV	0.024	0.60	0.107	0.064	0.80	0.113	0.053	0.68	0.074
OL	0.024	0.61	0.103	0.065	0.79	0.115	0.054	0.67	0.073

5.2.1 Tropical regions

In the tropics, all SMOS experiments (middle panels of Fig. 14) exhibit similar performance to the open loop, with errorbars indicating non-significant impacts. However, the experiments SMOS1-SLV, SMOS3-SLV and SMOS9-SLV show some small improvement for October-December and experiment SMOS9-SLV also for July-September. Experiments SMOS1 and SMOS3 show a small decrease of performance (increased RMS) in July-September. Even if errorbars are large, it is interesting to note that the experiments that show a slightly better forescast skill using only SMOS or SMOS+SLV are those with a higher observation error (and low weight of SMOS during the assimilation): SMOS9 and SMOS9-SLV, respectively Therefore, even if the effect is very small, it could be that SMOS NN SM degrades the forecast in the Tropics in the Northern hemisphere summer.

The experiments using ASCAT SM show an slightly different behaviour. Middle panels of Fig. 15 show a significant improvement of the forecast skill for experiments ASCAT1-SLV, ASCAT2-SLV and ASCAT4-SLV in particular in the period from July to December. In this case, the performance increase as the observation error of ASCAT SM decreases, giving more weight to ASCAT SM during the assimilation. In addition, even without SLVs, experiments ASCAT1 and ASCAT2 show a significant improvement of the forecast skill up to days 2-3 in July-December. Therefore, ASCAT SM improves the forecast in the tropics and adds information to the SLVs.

5.2.2 Southern hemisphere

Left panels of Figs. 14-15 show the results for the Southern Hemisphere. Experiments with SLVs show an improvement in the forecast both with SMOS and ASCAT for all the seasons except experiments with ASCAT (ASCATx-SLV) in July-September. Actually, experiments with ASCAT alone (in particular ASCAT1 and ASCAT2) degrade the forecast in the Northern hemisphere. Giving less weight to ASCAT (higher observation error, ASCAT4) the degradation is smaller. Therefore, ASCAT degrades the forecast in the Southern Hemisphere in July-September both alone and using SLVs.

In contrast, all experiments using SMOS and SLVs (SMOSx-SLV) improve the forecast for all the seasons, in particular, in July-December. The improvement is significant until days 4-5 in October-December. Both using only SMOS or SMOS+SLV, the forecast improvement increases as the observation error associated to SMOS decreases and the weight of SMOS in the assimilation increases (from SMOS9 to SMOS1 and from SMOS9-SLV to SMOS1-SLV). Results for experiment SMOS1 also show an improvement in the forecast in October-December and July-September for a shorter period. In July-September, the experiment SMOS3 also improve the forecast up to day 2. In conclusion, SMOS adds significant information to the SLVs and improves the forecast in the Southern Hemisphere mainly in the southern spring.

5.2.3 Northern Hemisphere

Left panels of Figs. 14-15 show the results for the Northern Hemisphere. Both with ASCAT and SMOS, experiments using SLVs improve the forecast in April-September. In both cases, the best scores are obtained when the observation errors is assumed to be low and the remote sensing data has a higher weight during the assimilation: experiments SMOS1-SLV (ASCAT1-SLV) performs better than SMOS9-SLV (ASCAT4-SLV). Therefore, both SMOS and ASCAT are adding information to the SLV. It is worth noting that due to the presence of snow, the amount of SM data in the Boreal winter is small. Experiments using ASCAT alone have a neutral impact except ASCAT1 and ASCAT2 in July-September, which have a small positive impact that could be significant (but the errorbars are almost reaching the RMSE = 0 line). In contrast, SMOS alone has a significant positive effect in July-September for experiments SMOS1 and SMOS3. The performance of SMOS1 is similar

to SMOS9-SLV, therefore, the impact of SMOS alone is similar to that the SLVs alone.

Figure 16 shows maps of the forecast skill for air temperature at 850 hPa averaged for the July-September period as a function of the forecast time from 12 to 72 hours. The six left panels (Fig. 16a) show the results for experiment SMOS3-SLV and the six right panels (Fig. 16b) show the results for experiment SMOS9-SLV, for which the weight given to SMOS NN SM is very low and it is close to a SLV-alone experiment. Comparing Fig. 16a and b, it is clear that SMOS improves the forecast in North America and to a lesser extend in Northern Asia up to 72 hours.

5.3 ASCAT and SMOS comparison

The results obtained in the current study show a complementarity of the SMOS and ASCAT data. This is not surprising as they are instruments of different nature (active/passive, C/L-Bands,...). Other studies using tripe collocation (Al-Yaari et al., 2014) or the merging approach of the Climate Change Initiative (Liu et al., 2011) also show a similar complementarity. More detailed studies at regional scale would be needed to fully understand this complementarity in the sensitivity of the atmosphere to the analysed surface fields using ASCAT or SMOS.

5.4 Comparison to the assimilation of SMOS brightness temperatures

A preliminary study of the impact of directly assimilating SMOS T_b's observations on soil moisture analysis and the atmospheric scores near the surface was presented at ECMWF by Muñoz-Sabater (2015). The results did not provide evidence of significant improvements of air temperature and air humidity, however they demonstrated to be beneficial for soil moisture analysis at the location of five stations of the SCAN network where the assimilation increments were high. In Muñoz-Sabater et al. (2016a) the SMOS observation error was calibrated to find a trade-off between surface skill and atmospheric skill. In addition, a more complete evaluation with respect to the USCRN and SCAN networks was presented. They showed that, on average, the assimilation of SMOS brightness temperatures does not improve significantly the soil moisture for those networks. In the current study, it has been shown that the analysis improves the soil moisture for some sites, in agreement with Muñoz-Sabater (2015). However, on average, the soil moisture analysis does not improve significantly the statistical scores when comparing to a large number of *in situ* sites, which is also in agreement with the results of Muñoz-Sabater et al. (2016a).

Regarding the sensitivity of the atmospheric forecast to SMOS brightness temperatures or SMOS NN SM assimilation, one should bear in mind the conceptual differences of the two approaches. In the first case, an observation operator is implemented within the assimilation scheme using a radiative transfer code. In the second case, the SMOS brightness temperatures are converted into the model variable using an statistical approach (NN) before the actual assimilation. In addition, there are important differences in the data assimilation set-up. The current study relies on an uncoupled DA in a 24 h window, while the Muñoz-Sabater et al. (2016a) study uses the IFS coupled approach in a 12 h DA window (see Table 3 for a comparison of so-LDAS and IFS-LDAS). Therefore, the current study should be considered as a research experiment to investigate the relative impact of soil moisture DA using three different observation types (SMOS NN SM, ASCAT SM, SLV), rather than for operational NWP purpose. The offline approach has the great advantage to enable at a reasonable computing cost such an extensive set of DA experiments. In addition it makes it possible to run one-year long DA experiments which ensure statistical robustness of the results. So, it provides a reliable insight on the relative impact of the different observation type DA and their combinations.

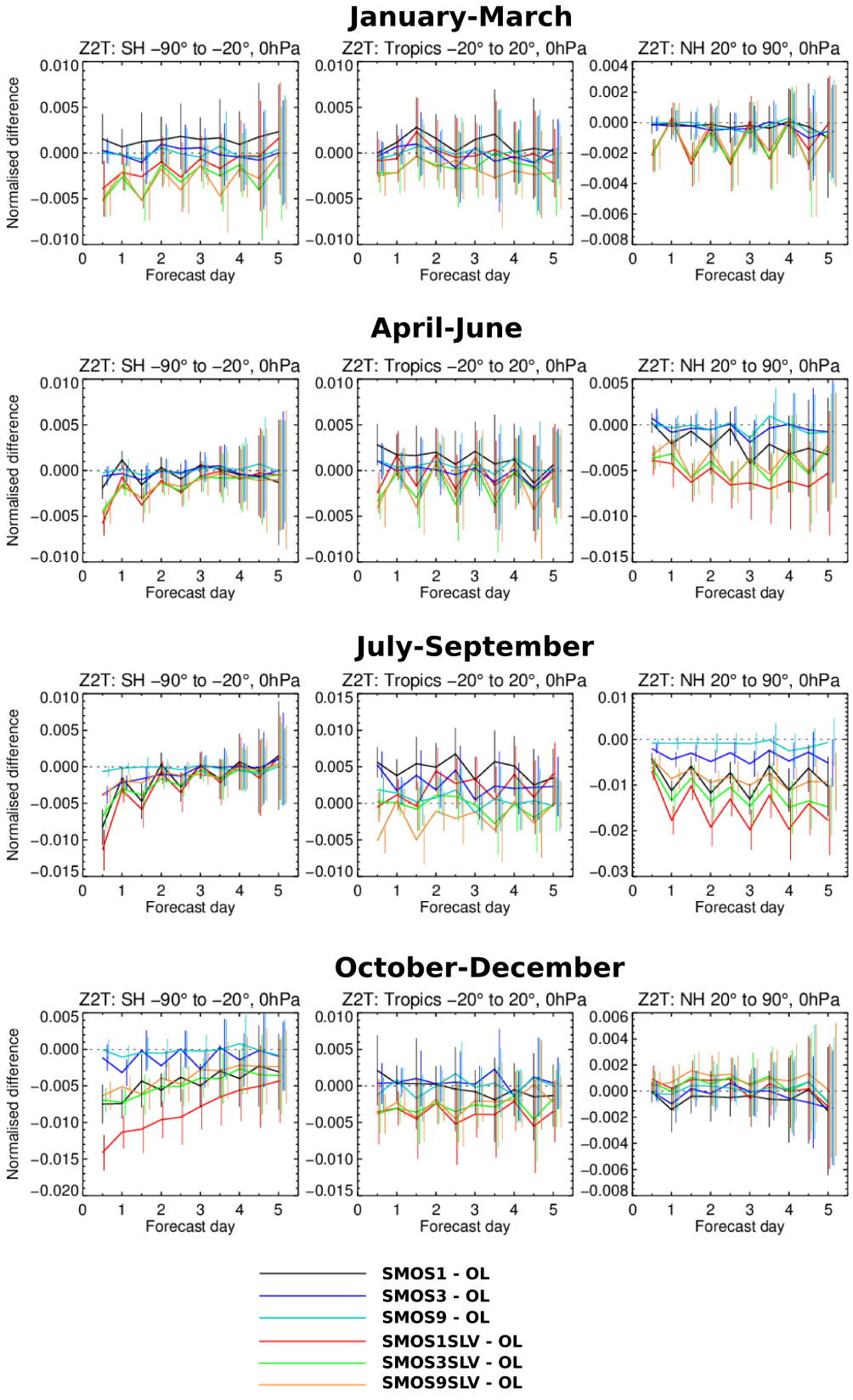

Figure 14: Evaluation of the atmospheric forecast skill for the SMOS assimilation experiments (RMSE of assimilation minus open-loop) as a function of time for T_{2m}. From top to bottom the three quarters of 2012 are shown. The results are shown for three latitude ranges: [-90°, -20°] (left panels), [-20°, 20°] (middle panels), [20°, 90°] (right panels).

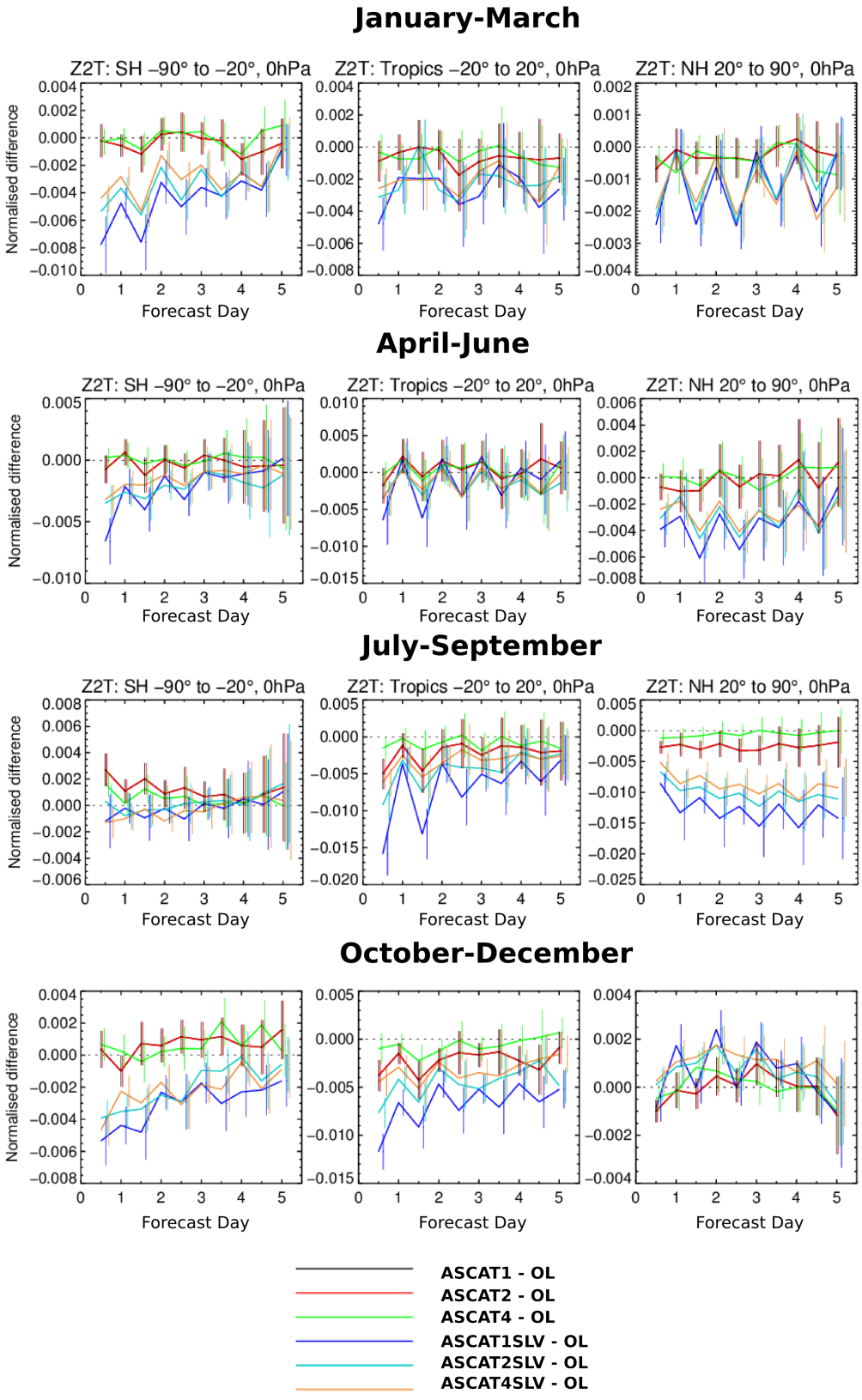

Figure 15: Evaluation of the atmospheric forecast skill for the ASCAT assimilation experiments (RMSE of assimilation minus open-loop) as a function of time for T_{2m}. From top to bottom the three quarters of 2012 are shown. The results are shown for three latitude ranges: [-90°, -20°] (left panels), [-20°, 20°] (middle panels), [20°, 90°] (right panels).

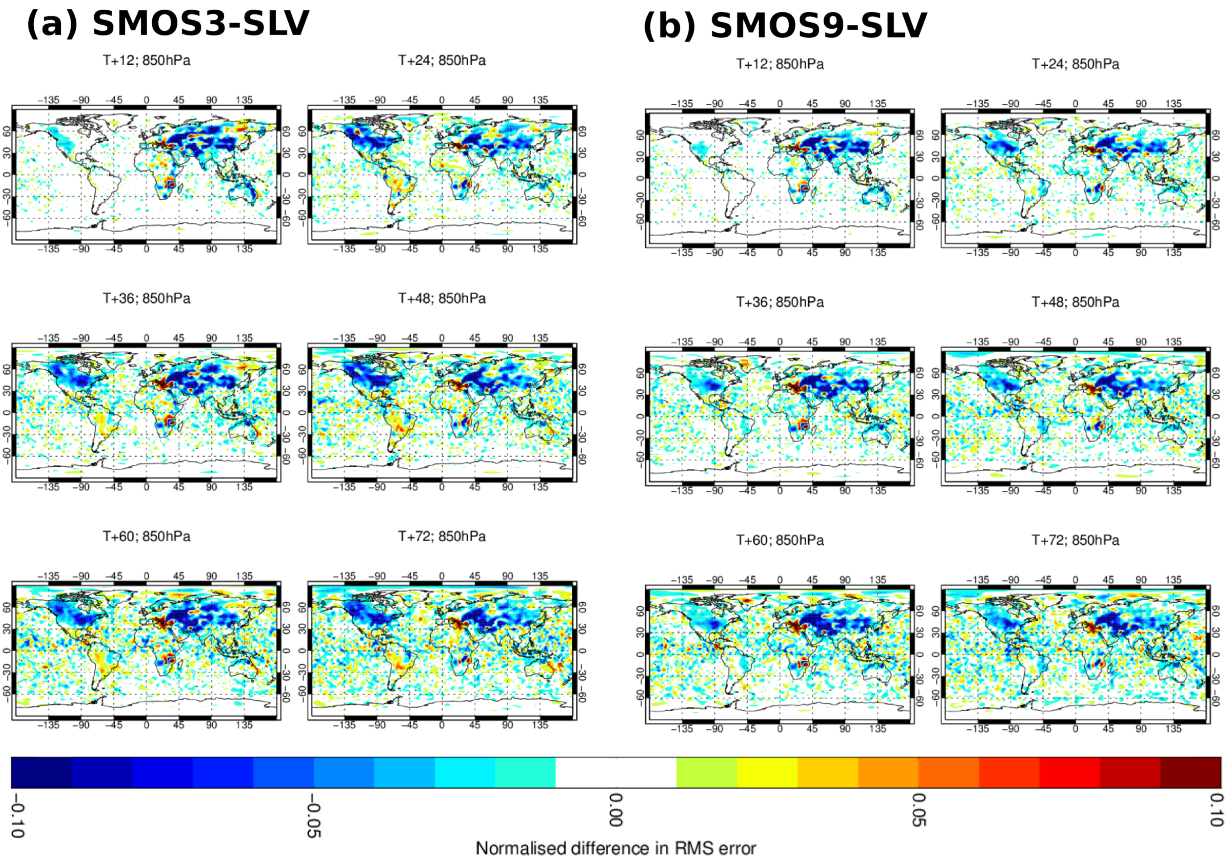

*Figure 16: Evaluation on the forecast skill for air temperature at 850 hPa as a function of time (from 12 to 72 hours). Average over July-September of the RMS difference of SMOS3-SLV (**a**) and SMOS9-SLV (**b**) with respect to the open loop (negative values, blue colors, are an improvement of the forecast skills).*

6 Summary and conclusions

A set of soil moisture data assimilation experiments was presented and evaluated for NWP applications. The experiments were computed using the HTESSEL land surface model and the offline so-LDAS (surface-only Land Data Assimilation System) in order to use a very computationally efficient system that allows to perform long surface assimilation experiments (e.g., one whole year, 2012). The analysis was done for soil moisture in the first three layers of the model using soil moisture retrievals by SMOS and ASCAT satellites and conventional 2 meters air temperature and relative humidity. ASCAT soil moisture was produced using the same approach used for the soil moisture analysis in the IFS which included a bias correction CDF-matching with respect to H-TESSEL. The SMOS soil moisture dataset was produced specifically for this project training a neural network using SMOS brightness temperatures as input and H-TESSEL soil moisture fields as reference for the training. In this way, the SMOS neural network soil moisture dataset has a similar climatology to the model and do not present a global bias with respect to the model. Several assimilation experiments were conducted using different observation errors for the ASCAT and SMOS datasets.

The different SM analyses were studied in the four quarters of 2012 and compared. Some seasonal effects and differences of experiments using SMOS and ASCAT were found. For instance cumulative increments for experiments using SMOS in Australia, South Africa and parts of South America are negative in October-March and they are positive from April to September. Interestingly, the seasonal analysis of the increments obtained when assimilating ASCAT SM also show seasonal patterns in those regions but they are shifted by three months since they are mainly negative from January to June and positive from July to December. Increments in July-September are positive in the Sahel when assimilating ASCAT SM while they are negative when assimilating SMOS NN SM. The increments in the first soil layer due to the assimilation of 2m air temperature and relative humidity are significant in the west of North America, central Asia, the Sahel and South Africa, part of the Amazon region, and Australia. In contrast to the remote sensing measurements of surface SM, the SLVs can constrain the SM content at deeper soil layers.

The different soil moisture analysed field were evaluated against a large number of in situ measurements of soil moisture. The SM analysis gives in general similar results to the model open loop with no assimilation. The choice of the observation error configuration, or the assimilated SM dataset have a relatively low impact on the analysed soil moisture (for the sites with in situ measurements) when looking at mean statistics.

Finally, the analysed soil moisture fields were used to initialise a set of atmospheric forecasts experiments to assess the impact on NWP performances. ASCAT soil moisture data assimilation improves the near-surface forecast in the tropics and adds information with respect to the screen level (conventional observations) data assimilation experiments. In contrast, SMOS data assimilation slightly degrades the forecast in the Tropics in July-September. In the Southern hemisphere experiments with SMOS or ASCAT combined with screen level observations show an improvement in the forecast for all the seasons except experiments with ASCAT in July-September. Actually, ASCAT degrades the forecast in the Southern Hemisphere in July-September both alone and combined with 2m air temperature and relative humidity. In contrast, all experiments using SMOS and SLVs improve the forecast for all the seasons, in particular, in July-December. Assimilation of SMOS soil moisture alone with a low observation error also shows an improvement in the forecast in July-December. Finally, in the Northern Hemisphere both with ASCAT and SMOS, the experiments using 2m air temperature and relative humidity improve the forecast in April-September. SMOS alone has a significant positive effect in July-September for experiments with low observation error. Maps of the forecast skill with respect to the open loop experiment show that SMOS improves the forecast in North America and to a lesser extend in Northern Asia for up to 72 hours.

In conclusion, an innovative technique that uses a neural network to construct a soil moisture dataset prior assimilation was discussed and evaluated. The experiments were compared to other ones using ASCAT soil

moisture. Differences have been shown and both instruments seem to provide complementary information. The results obtained for the assimilation of SMOS soil moisture are very promising as they show a clear impact in the forecast.

Further research will allow to evaluate SMOS and ASCAT data assimilation in an operational framework.

References

Aires, F. and C. Prigent, 2006: Toward a new generation of satellite surface products? *Journal of Geophysical Research: Atmospheres (1984–2012)*, 111 (D22).

Aires, F., C. Prigent, and W. B. Rossow, 2005: Sensitivity of satellite microwave and infrared observations to soil moisture at a global scale: 2. Global statistical relationships. *Journal of Geophysical Research*, 110 (D11).

Al-Yaari, A., et al., 2014: Global-scale comparison of passive (smos) and active (ascat) satellite based microwave soil moisture retrievals with soil moisture simulations (merra-land). *Remote Sensing of Environment*, 152, 614–626.

Albergel, C., G. Balsamo, P. d. Rosnay, J. Muñoz-Sabater, and S. Boussetta, 2012: A bare ground evaporation revision in the ecmwf land-surface scheme: evaluation of its impact using ground soil moisture and satellite microwave data. *Hydrology and Earth System Sciences*, 16 (10), 3607–3620.

Balsamo, G., A. Beljaars, K. Scipal, P. Viterbo, B. van den Hurk, M. Hirschi, and A. K. Betts, 2009: A revised hydrology for the ECMWF model: Verification from field site to terrestrial water storage and impact in the integrated forecast system. *Journal of hydrometeorology*, 10 (3), 623–643.

Balsamo, G., F. Bouyssel, and J. Noilhan, 2004: A simplified bi-dimensional variational analysis of soil moisture from screen-level observations in a mesoscale numerical weather-prediction model. *Quarterly Journal of the Royal Meteorological Society*, 130 (598), 895–915.

Balsamo, G., E. Dutra, S. Boussetta, A. Beljaars, P. Viterbo, and B. van den Hurk, 2010: Recent advances in land surface modelling at ecmwf. *ECMWF/GLASS workshop on Land Surface Modelling*, 9–12.

Balsamo, G., J. Mahfouf, S. Bélair, and G. Deblonde, 2007: A land data assimilation system for soil moisture and temperature: an information content study. *Journal of Hydrometeorology*, 8 (6), 1225–1242.

Balsamo, G., et al., 2015: ERA-Interim/Land: a global land surface reanalysis data set. *Hydrology and Earth System Sciences*, 19 (1), 389–407.

Bartalis, Z., W. Wagner, V. Naeimi, S. Hasenauer, K. Scipal, H. Bonekamp, J. Figa, and C. Anderson, 2007: Initial soil moisture retrievals from the METOP-A Advanced Scatterometer (ASCAT). *Geophysical Research Letters*, 34 (2), 20 401.

Bircher, S., N. Skou, K. H. Jensen, J. P. Walker, and L. Rasmussen, 2012: A soil moisture and temperature network for SMOS validation in Western Denmark. *Hydrology and Earth System Sciences*, 16 (5), 1445–1463.

Bircher, S., N. Skou, and Y. H. Kerr, 2013: Validation of SMOS L1C and L2 Products and Important Parameters of the Retrieval Algorithm in the Skjern River Catchment, Western Denmark. *IEEE Transactions on Geoscience and Remote Sensing*, 51(5), 2969–2985.

Blankenship, C. B., J. L. Case, B. T. Zavodsky, and W. L. Crosson, 2016: Assimilation of smos retrievals in the land information system. *IEEE Transactions on Geoscience and Remote Sensing*, 54 (11).

Boussetta, S., G. Balsamo, A. Beljaars, T. Kral, and L. Jarlan, 2013: Impact of a satellite-derived leaf area index monthly climatology in a global numerical weather prediction model. *International Journal of Remote Sensing*, 34 (9-10), 3520–3542.

Calvet, J.-C., N. Fritz, F. Froissard, D. Suquia, A. Petitpa, and B. Piguet, 2007: In situ soil moisture observations for the cal/val of smos: The smosmania network. *Geoscience and Remote Sensing Symposium, 2007. IGARSS 2007. IEEE International*, IEEE, 1196–1199.

Carrera, M., B. Bilodeau, A. Russell, X. Wang, and S. Belair, 2016: Towards the implementation of l-band soil moisture brightness temperatures in the canadian land data assimilation system (CaLDAS). *EGU General Assembly Conference Abstracts*, Vol. 18, 7520.

De Lannoy, G. J. and R. H. Reichle, 2016: Global assimilation of multiangle and multipolarization SMOS brightness temperature observations into the GEOS-5 catchment land surface model for soil moisture estimation. *Journal of Hydrometeorology*, 17 (2), 669–691.

de Rosnay, P., G. Balsamo, C. Albergel, J. Muñoz-Sabater, and L. Isaksen, 2014: Initialisation of land surface variables for numerical weather prediction. *Surveys in Geophysics*, 35 (3), 607–621.

de Rosnay, P., G. De Chiara, and I. Mallas, 2011: Use of ASCAT soil moisture: revised bias correction and test of improved ASCAT product in IFS cycle 37r2. Tech. Rep. R43.8/PdR/11100, ECMWF.

de Rosnay, P., M. Dragosavac, M. Drusch, A. Gutiérrez, M. Rodríguez López, N. Wright, J. Muñoz Sabater, and C. R., 2012: SMOS NRT BUFR specification. SMOS-NRT-BUFR-ECMWF - v2.0, ECMWF.

de Rosnay, P., M. Drusch, and J. M. Sabater, 2009: Milestone 1 Tech Note - Part 1: SMOS Global Surface Emission Model, Progress report for ESA contract 3-11640/06/I-LG. Tech. rep., ECMWF.

de Rosnay, P., M. Drusch, D. Vasiljevic, G. Balsamo, C. Albergel, and L. Isaksen, 2013: A simplified extended kalman filter for the global operational soil moisture analysis at ecmwf. *Quarterly Journal of the Royal Meteorological Society*, 139 (674), 1199–1213.

Dee, D., et al., 2011: The era-interim reanalysis: Configuration and performance of the data assimilation system. *Quarterly Journal of the Royal Meteorological Society*, 137 (656), 553–597.

Dorigo, W., et al., 2011: The international soil moisture network: a data hosting facility for global in situ soil moisture measurements. *Hydrology and Earth System Sciences*, 15 (5), 1675–1698.

Douville, H., P. Viterbo, J.-F. Mahfouf, and A. C. Beljaars, 2000: Evaluation of the optimum interpolation and nudging techniques for soil moisture analysis using fife data. *Monthly Weather Review*, 128 (6), 1733–1756.

Draper, C., J.-F. Mahfouf, and J. Walker, 2009: An EKF assimilation of AMSR-E soil moisture into the ISBA land surface scheme. *Journal of Geophysical Research: Atmospheres*, 114 (D20).

Drusch, M., 2007: Initializing numerical weather prediction models with satellite-derived surface soil moisture: Data assimilation experiments with ECMWF's integrated forecast system and the TMI soil moisture data set. *Journal of Geophysical Research: Atmospheres (1984–2012)*, 112 (D3).

Drusch, M., K. Scipal, P. De Rosnay, G. Balsamo, E. Andersson, P. Bougeault, and P. Viterbo, 2009: Towards a kalman filter based soil moisture analysis system for the operational ECMWF integrated forecast system. *Geophysical Research Letters*, 36 (10).

Drusch, M., E. Wood, and H. Gao, 2005: Observation operators for the direct assimilation of trmm microwave imager retrieved soil moisture. *Geophysical Research Letters*, 32 (15).

Gutierrez, A. and A. Canales Molina, 2010: SMOS NRT Product Format Specification. Tech. Rep. SO-ID-DMS-GS-0002, DEIMOS Space.

Kerr, Y., et al., 2010: The SMOS mission: New tool for monitoring key elements ofthe global water cycle. *Proceedings of the IEEE*, 98 (5), 666–687.

Kerr, Y., et al., 2013: Catds smos l3 soil moisture retrieval processor, algorithm theoretical baseline document (atbd). Tech. rep., CBSA Technical Note SO-TN-CBSA-GS-0029, Issue 2.0.

Koster, R. D., et al., 2004: Regions of strong coupling between soil moisture and precipitation. *Science*, 305 (5687), 1138–1140.

Leavesley, G., O. David, D. Garen, J. Lea, J. Marron, T. Pagano, T. Perkins, and M. Strobel, 2008: A modeling framework for improved agricultural water supply forecasting. *AGU Fall Meeting Abstracts*, Vol. 1, 0497.

Lievens, H., et al., 2016: Assimilation of smos soil moisture and brightness temperature products into a land surface model. *Remote Sensing of Environment*, 180, 292–304.

Liu, Y., R. Parinussa, W. Dorigo, R. De Jeu, W. Wagner, A. Van Dijk, M. McCabe, and J. Evans, 2011: Developing an improved soil moisture dataset by blending passive and active microwave satellite-based retrievals. *Hydrology and Earth System Sciences*, 15 (2), 425–436.

Mahfouf, J.-F., 1991: Analysis of soil moisture from near-surface parameters: A feasibility study. *Journal of applied meteorology*, 30 (11), 1534–1547.

Mahfouf, J.-F., K. Bergaoui, C. Draper, F. Bouyssel, F. Taillefer, and L. Taseva, 2009: A comparison of two off-line soil analysis schemes for assimilation of screen level observations. *Journal of Geophysical Research: Atmospheres*, 114 (D8).

Mahfouf, J.-F., P. Viterbo, H. Douville, A. Beljaars, and S. Saarinen, 2000: A revised land-surface analysis scheme in the integrated forecastingsystem. Tech. rep., ECMWF Newsletter No. 88.

Martens, B., D. Miralles, H. Lievens, D. Fernández-Prieto, and N. Verhoest, 2016: Improving terrestrial evaporation estimates over continental australia through assimilation of smos soil moisture. *International Journal of Applied Earth Observation and Geoinformation*, 48, 146–162.

Martínez-Fernández, J. and A. Ceballos, 2005: Mean soil moisture estimation using temporal stability analysis. *Journal of Hydrology*, 312 (1), 28–38.

Mecklenburg, S., et al., 2016: Esa's soil moisture and ocean salinity mission: From science to operational applications. *Remote Sensing of Environment*, 180, 3–18.

Muñoz-Sabater, J., 2015: Incorporation of passive microwave brightness temperatures in the ECMWF soil moisture analysis. *Remote Sensing*, 7 (5), 5758–5784.

Muñoz-Sabater, J., P. de Rosnay, C. Albergel, and L. Isaksen, 2016a: SMOS report on background and observation error scenarios. Tech. rep., ECMWF ESA /ESRIN contract 4000101703/10/NL/FF/fk, TNPII WP3401 & WP3402.

Muñoz-Sabater, J., N. J. Rodríguez-Fernández, P. Richaume, P. de Rosnay, and Y. H. Kerr, 2016b: SMOS Near-Real-Time Soil Moisture processor. Tech. Rep. ECMWF ESA report, ECMWF, Reading, UK.

Noilhan, J. and J.-F. Mahfouf, 1996: The ISBA land surface parameterisation scheme. *Global and planetary Change*, 13 (1), 145–159.

Noilhan, J. and S. Planton, 1989: A simple parameterization of land surface processes for meteorological models. *Monthly Weather Review*, 117 (3), 536–549.

Parrens, M., J.-F. Mahfouf, A. Barbu, and J.-C. Calvet, 2014: Assimilation of surface soil moisture into a multilayer soil model: design and evaluation at local scale. *Hydrology and Earth System Sciences*, 18 (2), 673–689.

Ridler, M.-E., H. Madsen, S. Stisen, S. Bircher, and R. Fensholt, 2014: Assimilation of smos-derived soil moisture in a fully integrated hydrological and soil-vegetation-atmosphere transfer model in western denmark. *Water Resources Research*, 50 (11), 8962–8981.

Rodríguez-Fernández, N. J., P. Richaume, J. Muñoz-Sabater, P. de Rosnay, and Y. H. Kerr, 2016: SMOS Near-Real-Time Soil Moisture processor. Operational implementation and product evaluation. Tech. Rep. SMOS Ground Segment SO-TN-CB-GS-049, CESBIO, Toulouse, France.

Rodríguez-Fernández, N. J., et al., 2015: Soil moisture retrieval using neural networks: application to SMOS. *IEEE Transactions on Geoscience and Remote Sensing*, Volume:53 , Issue: 11, 5991–6007.

Schaefer, G., M. Cosh, and T. Jackson, 2007: The USDA natural resources conservation service soil climate analysis network (SCAN). *Journal of Atmospheric and Oceanic Technology*, 24 (12), 2073–2077.

Scholze, M., T. Kaminski, W. Knorr, S. Blessing, M. Vossbeck, J. Grant, and K. Scipal, 2016: Simultaneous assimilation of smos soil moisture and atmospheric co 2 in-situ observations to constrain the global terrestrial carbon cycle. *Remote Sensing of Environment*, 180, 334–345.

Scipal, K., M. Drusch, and W. Wagner, 2008: Assimilation of a ers scatterometer derived soil moisture index in the ECMWF numerical weather prediction system. *Advances in water resources*, 31 (8), 1101–1112.

Seneviratne, S. I., T. Corti, E. L. Davin, M. Hirschi, E. B. Jaeger, I. Lehner, B. Orlowsky, and A. J. Teuling, 2010: Investigating soil moisture–climate interactions in a changing climate: A review. *Earth-Science Reviews*, 99 (3), 125–161.

Seuffert, G., H. Wilker, P. Viterbo, M. Drusch, and J. Mahfouf, 2004: The usage of screen-level parameters and microwave brightness temperature for soil moisture analysis. *Journal of Hydrometeorology*, 5 (3), 516–531.

Tagesson, T., et al., 2015: Ecosystem properties of semiarid savanna grassland in west africa and its relationship with environmental variability. *Global Change Biology*, 21 (1), 250–264.

Tuttle, S. and G. Salvucci, 2016: Empirical evidence of contrasting soil moisture–precipitation feedbacks across the united states. *Science*, 352 (6287), 825–828.

van den Hurk, B., A. C. M. Beljaars, and A. K. Betts, 2000: Offline validation of the era-40 surface scheme. *ECMWF Tech. Memo. 295*, 43 pp.

Weisheimer, A., F. J. Doblas-Reyes, T. Jung, and T. Palmer, 2011: On the predictability of the extreme summer 2003 over europe. *Geophysical Research Letters*, 38 (5).

Xu, X., B. A. Tolson, J. Li, R. M. Staebler, F. Seglenieks, A. Haghnegahdar, and B. Davison, 2015: Assimilation of smos soil moisture over the great lakes basin. *Remote Sensing of Environment*, 169, 163–175.